Development 140, 1693-1702 (2013) doi:10.1242/dev.089656
© 2013. Published by The Company of Biologists Ltd

A Cul-3-BTB ubiquitylation pathway regulates junctional levels and asymmetry of core planar polarity proteins

Helen Strutt*, Elizabeth Searle*, Victoria Thomas-MacArthur, Rosalind Brookfield and David Strutt‡

SUMMARY

The asymmetric localisation of core planar polarity proteins at apicolateral junctions is required to specify cell polarity in the plane of epithelia. This asymmetric distribution of the core proteins is proposed to require amplification of an initial asymmetry by feedback loops. In addition, generation of asymmetry appears to require the regulation of core protein levels, but the importance of such regulation and the underlying mechanisms is unknown. Here we show that ubiquitylation acts through more than one mechanism to control core protein levels in *Drosophila*, and that without this regulation cellular asymmetry is compromised. Levels of Dishevelled at junctions are regulated by a Cullin-3-Diablo/Kelch ubiquitin ligase complex, the activity of which is most likely controlled by neddylation. Furthermore, activity of the deubiquitylating enzyme Fat facets is required to maintain Flamingo levels at junctions. Notably, ubiquitylation does not alter the total cellular levels of Dishevelled or Flamingo, but only that of the junctional population. When junctional core protein levels are either increased or decreased by disruption of the ubiquitylation machinery, their asymmetric localisation is reduced and this leads to disruption of planar polarity at the tissue level. Loss of asymmetry by altered core protein levels can be explained by reference to feedback models for amplification of asymmetry.

KEY WORDS: Planar polarity, PCP, Ubiquitination, Neddylation, Dishevelled, *Drosophila*

INTRODUCTION

Polarisation of cells in the plane of an epithelium is essential for morphogenesis and depends on a group of core planar polarity proteins (the 'core proteins'), the function of which is conserved among diverse animal species. The core proteins localise asymmetrically within cells, and this asymmetric localisation regulates downstream processes such as polarised cell rearrangements, oriented cell divisions and the production of uniformly oriented arrays of structures such as hairs and cilia (McNeill, 2010; Goodrich and Strutt, 2011; Gray et al., 2011; Vichas and Zallen, 2011). The function of the core proteins has been best studied in the *Drosophila* wing. Here, the core proteins Frizzled (Fz), Dishevelled (Dsh) and Diego (Dgo) localise at the distal cell edge, whereas Strabismus (Stbm, also known as Van Gogh) and Prickle (Pk) localise proximally and Flamingo (Fmi, also known as Starry night) localises at both edges. This leads to the formation of an actin-rich trichome at the distal cell edge.

A key question is how the asymmetric localisation of core proteins is achieved. Correct asymmetry depends on the activity of all the other core proteins, and it is thought that an initial asymmetry on the proximodistal (PD) axis caused by an upstream cue is amplified by feedback interactions between the core proteins (Tree et al., 2002; Amonlirdviman et al., 2005; Le Garrec et al., 2006; Meinhardt, 2007). Feedback loops operate as bistable switches, enhancing the initially weak PD bias in core protein distribution, such that core proteins ultimately show high asymmetry in their localisation to the proximal and distal cell edges, and low levels of localisation on the anterior-posterior (AP) cell edges. Feedback could be caused by either positive or negative protein interactions: for instance, a possible positive interaction would be clustering of asymmetric complexes of the same polarity (Strutt et al., 2011), whereas inhibition between proximal and distal complex components would constitute a negative interaction (Tree et al., 2002; Jenny et al., 2005).

Interestingly, asymmetrically localised core proteins are not uniformly localised on the PD cell membranes but are instead organised in discrete puncta (Aigouy et al., 2010; Strutt et al., 2011), and the presence and size of these puncta correlate with the degree of asymmetry. We have previously provided evidence that they form by a two-step mechanism: first, a stable complex forms with Fz and Fmi on one side of the junctions and Stbm and Fmi on the other; second, the cytoplasmic components cause these stable complexes to congregate into discrete membrane subdomains (Strutt et al., 2011). Therefore, the activity of the cytoplasmic proteins appears to be a crucial feature of the feedback loops necessary to generate asymmetry.

It also appears that overall core protein levels must be regulated, as overexpression of the cytoplasmic proteins (Dsh, Pk and Dgo) causes excessive accumulation of the other core proteins at junctions and a loss of asymmetry (Feiguin et al., 2001; Tree et al., 2002; Bastock et al., 2003). In theory, both positive- and negative-feedback interactions require that core protein levels are modulated. For example, an excess of one or more core proteins could disrupt both positive interactions (by causing clustering to spread beyond the required domain) and negative interactions (by an excess of inhibition excluding competitor proteins from an increased proportion of membrane domains). Despite this, the degree to which asymmetry is dependent on the levels of core proteins at junctions has not been studied. In addition, it is not known whether it is the levels of all or of just some of the core proteins that must be regulated.

MRC Centre for Developmental and Biomedical Genetics and Department of Biomedical Science, University of Sheffield, Western Bank, Sheffield S10 2TN, UK.

*These authors contributed equally to this work
‡Author for correspondence (d.strutt@sheffield.ac.uk)

This is an Open Access article distributed under the terms of the Creative Commons Attribution Non-Commercial Share Alike License (http://creativecommons.org/licenses/by-nc-sa/3.0), which permits unrestricted non-commercial use, distribution and reproduction in any medium provided that the original work is properly cited and all further distributions of the work or adaptation are subject to the same Creative Commons License terms.

Accepted 4 February 2013

One mechanism by which cellular levels of proteins can be regulated is ubiquitylation, which can lead to either the proteasomal degradation of cytoplasmic proteins or the targeting of transmembrane proteins for internalisation and degradation in the lysosome (Hershko and Ciechanover, 1998; Traub and Lukacs, 2007; Clague et al., 2012). Fz and Dsh also act in canonical Wnt signalling and, interestingly, are known to be regulated by ubiquitylation in this context. In flies, Fz levels are modulated by the deubiquitylating enzyme dUBPY (Mukai et al., 2010), and in vertebrates Dsh homologues are regulated by ubiquitylation pathways involving KLHL12 and Cyld (Angers et al., 2006; Tauriello et al., 2010). However, no studies have described a role for ubiquitylation in regulating Fz and Dsh levels in planar polarity. Only one ubiquitylation pathway affecting planar polarity has been reported, which involves recruitment of murine Smurf2 to junctions by phosphorylated Dsh, leading to local degradation of Pk (Narimatsu et al., 2009). Other mechanisms by which ubiquitylation might regulate core protein levels and asymmetry *in vivo* are yet to be identified.

Ubiquitylation of target proteins requires the sequential action of a cascade of E1, E2 and E3 enzymes (Hershko and Ciechanover, 1998). Ubiquitin is directly conjugated to the E2 enzyme via E1 enzyme activity, and the E3 ligase then transfers ubiquitin to a lysine residue within the target protein. In addition to ubiquitylation, proteins can be modified by the conjugation of several other ubiquitin-like molecules. Nedd8 is one such molecule, and it is attached to substrates using a similar E1, E2 and E3 enzyme cascade (Rabut and Peter, 2008). Neddylation can alter protein stability or activity, and the best characterised targets of neddylation are Cullin E3 ligases. Neddylation promotes recruitment of the E2 enzyme to Cullins, and cycles of neddylation and deneddylation are required for proper functioning of Cullins (Wu et al., 2005).

Here, we characterise two distinct ubiquitylation pathways, which act through the core proteins Dsh and Fmi. Both loss of ubiquitylation and increased ubiquitylation alter core protein levels at junctions and reduce core protein asymmetry. Furthermore, we show that ubiquitylation does not affect the entire cellular pool of Fmi and Dsh, but only the junctional population.

MATERIALS AND METHODS

Fly stocks and genetics

Fly stocks are described in FlyBase. fz^{P21}, $stbm^{6}$, $pk^{pk\text{-}sple13}$, dsh^{V26}, dgo^{380}, faf^{BX4}, faf^{F08}, lqf^{7F1} and kel^{DE1} are null alleles. $Cul\text{-}3^{gft2}$ is a loss-of-function allele and $Nedd8^{AN015}$, fz^{N21} and fz^{J22} are hypomorphs. faf^{7F1} is a semi-viable EMS-induced hypomorphic allele (this work) and $dor^{JR\text{-}33733}$ is a GD RNAi line (VDRC).

Transgenes used were *ArmP-fmi-EGFP* (Strutt et al., 2011) and *ActP-FRT-polyA-FRT-dsh-ECFP* (Strutt and Strutt, 2007). *UAS-Myc-dbo*, *ActP-FRT-polyA-FRT-Myc-dbo* and *ActP-FRT-polyA-FRT-faf-EGFP* express Myc-tagged Dbo and Faf tagged at its C-terminus with EGFP using the vectors *pUAST* and *pActP-FRT-polyA-FRT*. The $dbo^{\Delta 25.1}$ knockout is a deletion of the entire open reading frame by homologous recombination using the *pRK2* vector as described (Huang et al., 2008). *dbo* small hairpin RNAi (shRNAi) lines contain 21-mer sequences of *dbo* (CGAGCGTTATGATCCACAAAC and CACTGAACTAAATATGCTACG) in *pVALIUM-20* (Ni et al., 2011) and do not overlap with each other or $dbo^{IR\text{-}105407}$.

Mitotic clones were induced using the FLP/FRT system and *Ubx-FLP*. Clones of *ActP-FRT-polyA-FRT-Myc-dbo* were made using *Ubx-FLP* and *Δ2-3*. Overexpression of *UAS-Myc-dbo* or RNAi lines used the GAL4/UAS system with *ptc-GAL4*. For pupal wing stainings, larvae expressing *Ubc12*, *Uba3* and *Roc1a* RNAi were raised at 18°C, and shifted to 29°C at 0 hours after prepupa formation (APF), whereas larvae expressing *Cul-3*, *dbo*, *kel* and *faf* RNAi were raised at 25°C and shifted to 29°C at 0 hours APF.

Transgenics were generated by Bestgene, Genetivision and Genetic Services.

RNAi screening

For the E2 screen, 32 genes encoding E2 ubiquitin ligases were identified by the presence of the ubiquitin conjugating enzyme E2 domain (IPR000608) within a predicted open reading frame. This correlates with the number of *D. melanogaster* genes analysed in a study of the evolution of the E2 gene family in metazoans (Michelle et al., 2009). The initial screen was carried out using GD lines from the VDRC or RNAi lines from NIG-FLY, but KK lines were subsequently screened when they became available.

BTB-encoding genes were selected based on the presence of a BTB/POZ domain (IPR013069). Additional RNAi lines for genes containing a BTB/Kelch-associated domain (IPR011705), Kelch repeat type 1 (IPR006652), Kelch repeat type 2 (IPR011498) or Kelch-type beat propeller (IPR015915) were also screened.

In the adult wing screens, RNAi lines were crossed to *MS1096-GAL4* virgins at 29°C. Male wings were mounted, unless the insertion was on the X chromosome, or as stated. For the pupal wing screens, RNAi lines were crossed to *ptc-GAL4* and raised at 18°C until 0 hours APF when white prepupae were collected and aged at 29°C for 26 hours before dissection and immunostaining with antibodies against Fmi and E-cadherin (Ecad; Shotgun – FlyBase).

Immunolabelling

Pupal wings were dissected at 28 hours APF at 25°C or at 25-26 hours at 29°C and imaged as previously (Strutt, 2001). Primary antibodies used were 1.5 μg/ml mouse anti-Fmi 74 [DSHB (Usui et al., 1999)], 1/300 rabbit anti-Fz (Bastock and Strutt, 2007), 1/1000 rat anti-Stbm (Strutt and Strutt, 2008), 1/1000 rat anti-Dsh (Strutt et al., 2006), 1/20 rat anti-Ecad [DSHB (Oda et al., 1994)], 1/2500 guinea pig anti-Senseless (Sens) (Nolo et al., 2000), 1/100 rabbit anti-Distalless (Dll) (Panganiban et al., 1995), 1/400 mouse anti-β-gal (Promega), 1/4000 rabbit anti-β-gal (Cappel), 1/4000 rabbit anti-GFP (Abcam) and 40 μg/ml mouse anti-Myc 9E10 (DSHB). A rabbit anti-Dsh serum (1/1000) was directed against amino acids 480-623, and a rat anti-Pk antibody (1/25) was directed against amino acids 514-769 and affinity purified. Phalloidin-A568 (1/100) was from Molecular Probes.

Biochemistry and western analysis

Venus-Cul3, Myc-Dbo and Myc-Kelch fusions were made in *pAVW* and *pAMW* Gateway vectors and also shuttled into *pcDNA3.1* (Invitrogen). Myc-Dbo deletions are of amino acids 72-169 (DboΔBTB), 174-276 (DboΔBACK), 323-end (DboΔKR) and 370-end (DboΔKR2-6) and are in *pAc5.1* (Invitrogen). Dsh-ECFP is in *pAc5.1* and EGFP-Dsh is in *pEGFP-C1* (Clontech).

For Cul-3-Dbo pulldowns, S2 cell lysates were made in RIPA buffer [50 mM Tris-HCl pH 7.5, 150 mM NaCl, 1% NP40, 0.5% Na deoxycholate, 0.1% SDS, 1× protease inhibitor cocktail (Roche)]. Pulldowns used goat anti-Myc agarose (Abcam). For Dbo-Dsh pulldowns, S2 or COS-7 cells were treated with 10 μM MG132 for 5 hours prior to making lysates in IP buffer [20 mM Tris-HCl pH 7.5, 150 mM NaCl, 0.5% Triton X-100, 1 mM Na_3VO_4, 5 mM NaF, 1× protease inhibitor cocktail (Roche)]. Immunoprecipitations used rabbit anti-GFP serum (Abcam) and protein G Sepharose (Xerxes). Westerns were probed with 1/2000 rabbit anti-GFP (Abcam), 1/1000 mouse anti-GFP JL8 (Clontech) or 0.2 μg/ml mouse anti-Myc 9E10 (DSHB).

For pupal wing westerns, 28-hour pupal wings were dissected into sample buffer, and one pupal wing equivalent was loaded per lane. Westerns were probed with 1.5 μg/ml mouse anti-Fmi 74 (DSHB), 1/200 rabbit anti-Dsh (this work), or 1/5000 Actin AC-40 mouse antibody (Sigma), and imaged on a UVIprochemie gel documentation system (UVItec). Bands from westerns of three biological replicates were quantitated in ImageJ (NIH).

Quantitation of protein levels and asymmetry at junctions

RNAi lines were expressed using the *MS1096-GAL4* driver. Wings were fixed and immunostained in parallel, and the same region of the wing was imaged at the same magnification and settings. To measure asymmetry, a 400×400 pixel region was selected and ImageJ used to mark a five pixel

line on all junctions (~200 per wing). The mean intensity and angle of each junction were measured, and a background value (non-junctional staining) subtracted. Excel (Microsoft) was used to bin angles into two categories: >45° (PD junctions) and <45° (AP junctions) from horizontal. The mean intensity of staining at PD and AP junctions was then calculated. Measurements were taken from eight wings of each genotype and the significance was determined using an unpaired *t*-test.

To compare absolute levels of junctional protein, a threshold value for wild-type images was empirically determined that highlighted the junctions, such that 4-5% of the image was above the threshold. The same threshold value was applied to the *Ubc12*, *Cul-3* and *faf* images. Overall intensity was mean intensity above the threshold (with background subtracted) multiplied by area above the threshold. Measurements were taken from at least eight wings of each genotype and the significance was determined using an unpaired *t*-test.

RESULTS

Regulation of core proteins by ubiquitylation and neddylation

In a genetic screen for enhancers of a hypomorphic *fz* phenotype in the *Drosophila* eye (Strutt and Strutt, 2003), we identified a new allele of *fat facets* (*faf*) (supplementary material Fig. S1A-D), which encodes a deubiquitylating enzyme (Huang et al., 1995). Ommatidia in *faf* mutant eye clones often contain extra photoreceptors due to defective Notch-Delta signalling (Overstreet et al., 2004), but in ommatidia with normal numbers of photoreceptor cells planar polarity defects were also observed (supplementary material Fig. S1E,F). Furthermore, in clones of cells lacking *faf* activity in the pupal wing, levels of all core proteins at apicolateral junctions were reduced (Fig. 1A-E), whereas levels of adherens junction proteins were unaffected (supplementary material Fig. S1G). In photoreceptor recruitment, Faf acts by deubiquitylating the Epsin Liquid facets (Lqf) (Chen et al., 2002). However, loss of *lqf* did not cause a decrease in the levels of any of the core proteins (Fig. 1F; data not shown), suggesting that the effect of *faf* on core proteins was independent of *lqf*.

To identify ubiquitylation pathways acting on the core proteins, we carried out an *in vivo* RNAi screen. We focused on E2 enzymes, as there are only 32 E2s in the *Drosophila* genome (Michelle et al., 2009), whereas there is a single ubiquitin E1 enzyme and several hundred putative E3 ligases. RNAi lines against a single E2, *Ubc12*, showed the reciprocal phenotype to that of *faf* in the pupal wing: an increase in core protein levels at apicolateral junctions (Fig. 1G-L; supplementary material Table S1).

Ubc12 does not encode a conventional ubiquitin E2, but the E2 for the related small modifying protein Nedd8 (Rabut and Peter, 2008). Other components of the Nedd8 pathway were therefore examined for effects on core protein levels. RNAi against the Nedd8 E1 subunit *Uba3* and the Nedd8 E3 subunit *Roc1a* also showed an increase in core protein levels (Fig. 1M,N; supplementary material Table S2), as did mutant clones of *Nedd8* itself (Fig. 1O,P).

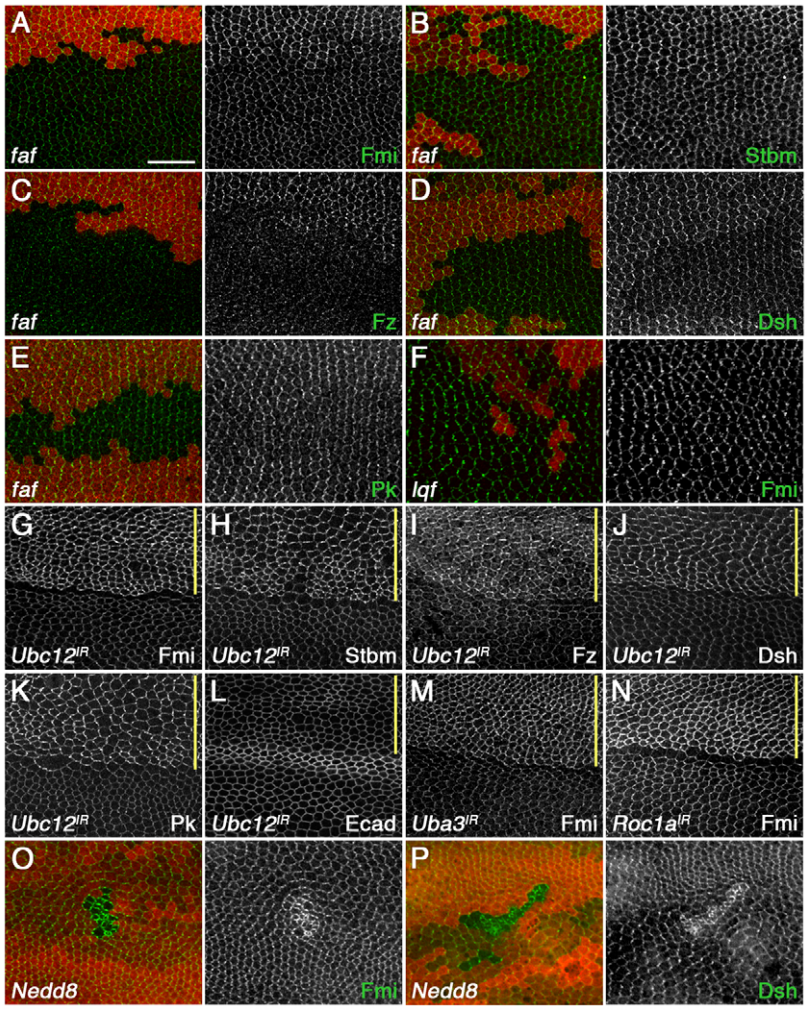

Fig. 1. Regulation of core proteins in *Drosophila* by ubiquitylation and neddylation. (**A-E**) faf^{8X4} clones. (**F**) lqf^{7F1} clone. (**G-N**) $Ubc12^{IR\text{-}7573R\text{-}3}$ (G-L), $Uba3^{IR\text{-}17139}$ (M) and $Roc1a^{IR\text{-}32399}$ (N), expressed with *ptc-GAL4*. (**O**,**P**) $Nedd8^{\Delta N015}$ clones. Immunostaining is for Fmi (green in A,F,G,M-O), Stbm (green in B,H), Fz (green in C,I), Dsh (green in D,J,P), Pk (green in E,K) and Ecad (green in L). Clones are marked by loss of β-gal (A-F) or GFP (O,P) in red. The band of stronger staining in L is the wing vein. Note the poor proliferation and small cells in *Nedd8* clones (O,P). The small lower clone in P does not show an increase in Dsh staining and cell size is normal, probably because it was induced late and there is perdurance of *Nedd8* activity. Yellow bars mark the *ptc-GAL4* domain. Scale bar: 20 μm.

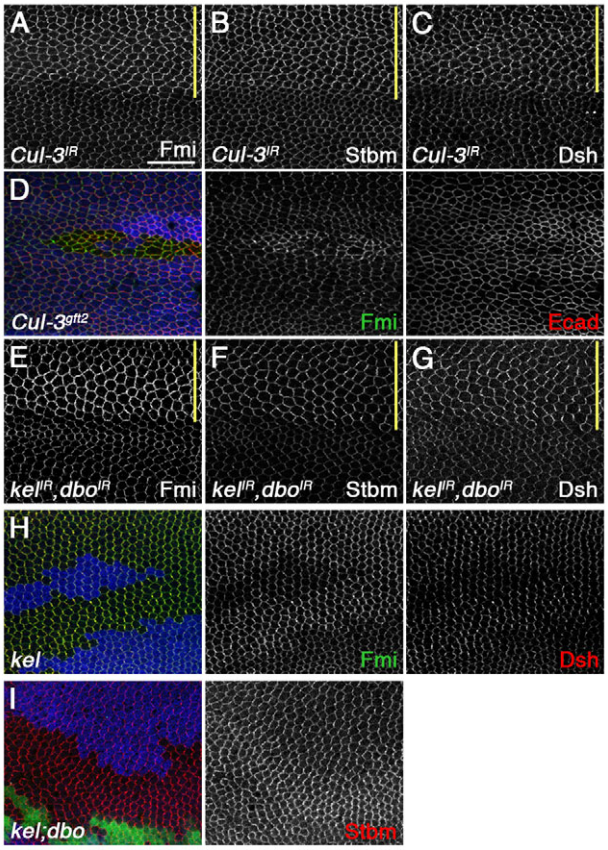

Fig. 2. A Cul-3-BTB protein complex regulates core protein levels. (**A-C**) *ptc-GAL4/Cul-3*$^{IR\text{-}109415}$. (**D**) *Cul-3*^{gft2} clone. (**E-G**) *ptc-GAL4/dbo*$^{IR\text{-}105407}$; *kel*$^{IR\text{-}JF01768}$*/UAS-Dcr2*. (**H**) *kel*^{DE1} clone. Immunostaining is for Fmi (A,D,E,H), Stbm (B,F), Dsh (C,G,H) and Ecad (D). Clones are marked by loss of β-gal (blue). Note the poor proliferation in the *Cul-3*^{gft2} clone (D). (**I**) Pupal wing with *kel*^{DE1} clones [marked by loss of GFP (green) staining] and overlapping *dbo*$^{\Delta 25.1}$ clones [marked by loss of β-gal (blue)], stained for Stbm (red): most of the tissue is mutant for *kel*, and there is an increase in Stbm staining in tissue that is also mutant for *dbo*. Yellow bars mark the *ptc-GAL4* domain. Scale bar: 20 μm.

A Cul-3-BTB E3 ubiquitin ligase complex regulates core protein levels and is the likely target of neddylation

One or more of the core proteins could be directly neddylated, or the effect of the Nedd8 pathway could be indirect via neddylation of another target. The best characterised substrates of Nedd8 are Cullin E3 ubiquitin ligases (Rabut and Peter, 2008). RNAi against *Cullin-3* (*Cul-3*), but none of the other Cullins, caused an increase in core protein levels at junctions, as did *Cul-3* null mutant clones (Fig. 2A-D; supplementary material Table S3). As Cul-3 is known to be modified by Nedd8 in flies (Wu et al., 2005), this suggests that Cul-3 is the likely target of Nedd8 in this context.

Cul-3 E3 ligase subunits act through substrate-specific partners of the BTB (BR-C, ttk and bab) family (Petroski and Deshaies, 2005). Screening of BTB proteins in the pupal wing (supplementary material Table S4) revealed that knockdown of *diablo* (*dbo*) and *kelch* (*kel*), which encode closely related Kelch family BTB proteins, caused subtle increases in core protein levels at apical junctions (supplementary material Fig. S2A-C). Simultaneous knockdown of *dbo* and *kel* caused a robust increase in core protein levels at junctions, suggesting that these two proteins act redundantly (Fig. 2E-G; compare with supplementary material Fig. S2A,C). *kel* null mutant animals are viable but female sterile (Schüpbach and Wieschaus, 1989), with no defects in trichome polarity (data not shown). However, core protein levels at junctions increased in *kel* mutant clones, consistent with the RNAi phenotype (Fig. 2H). We ruled out off-target effects for *dbo* in two ways. First, we generated two independent small hairpin RNAi (shRNAi) lines (Ni et al., 2011): both showed an increase in core protein levels at junctions when co-expressed with a *kel* RNAi line, but not when expressed alone (supplementary material Fig. S2D-G). Second, we knocked out the *dbo* open reading frame by homologous recombination: like *kel* mutants, *dbo* mutants were viable, with no trichome polarity phenotype (data not shown). No increase in core protein levels was observed in *dbo* mutant clones, possibly owing to perdurance of protein (supplementary material Fig. S2H), but induction of overlapping *dbo* and *kel* clones revealed that loss of both *kel* and *dbo* caused a greater increase in core protein levels than loss of *kel* alone (Fig. 2I).

Cul-3 binds to Kel in tissue culture (Hudson and Cooley, 2010): we confirmed this, finding that both Dbo and Kel were binding partners of Cul-3 in *Drosophila* S2 cells (Fig. 3B). Cul-3 binds to BTB proteins via their BTB and BACK domains (Petroski and Deshaies, 2005). Consistent with this, the Dbo-Cul-3 interaction depended on the BTB and BACK domains of Dbo, but not the Kelch repeats (Fig. 3C).

Regulation of core protein levels at junctions via ubiquitylation pathways is required for robust asymmetry

Although defects in ubiquitylation alter core protein levels at junctions, it is not clear whether this is important for asymmetry and trichome polarity. We therefore quantitated core protein asymmetry in pupal wings in which ubiquitylation was altered. For *Ubc12*, *Cul-3* and *faf*, RNAi lines were expressed ubiquitously in the wing using the *MS1096-GAL4* driver: this caused clear alterations in core protein levels compared with a control RNAi line, similar to that seen using *ptc-GAL4* (supplementary material Fig. S3A-E). Overall asymmetry was reduced by 35-50% when protein levels at junctions were increased by expression of *Ubc12* and *Cul-3* RNAi (Fig. 3D; supplementary material Fig. S3A-C) or in *kel; dbo* double-mutant wings (Fig. 3E; supplementary material Fig. S3F,G), or when protein levels were decreased by loss of *faf* activity (Fig. 3D; supplementary material Fig. S3D,E). In addition, cell packing was disrupted (supplementary material Fig. S3H); this might be a consequence of reduced asymmetry of the core proteins (Classen et al., 2005), or it could be due to effects of altered ubiquitylation that are independent of core proteins. Notably, cell packing was essentially normal in *faf* wings, even though core protein asymmetry was reduced, suggesting that the change in core protein asymmetry is not an indirect result of defects in cell packing. Thus, tight regulation of junctional core protein levels appears to be necessary for maximal cellular asymmetry.

It is known that the mechanisms leading to trichome placement are very robust, and trichomes can form at the correct cell edge in wings in which there is little or no visible asymmetry of core protein localisation, such as in *pk* or *dgo* mutants (Strutt and Strutt, 2007), apparently due to downstream amplifying mechanisms. Consistent with this, loss of *faf* activity delayed trichome formation (supplementary material Fig. S3I), but trichome orientation was normal (supplementary material Fig. S3J). However, *kel; dbo* double mutants showed localised trichome swirling in the wing (Fig. 3F) and occasional defects in ommatidial polarity in the eye

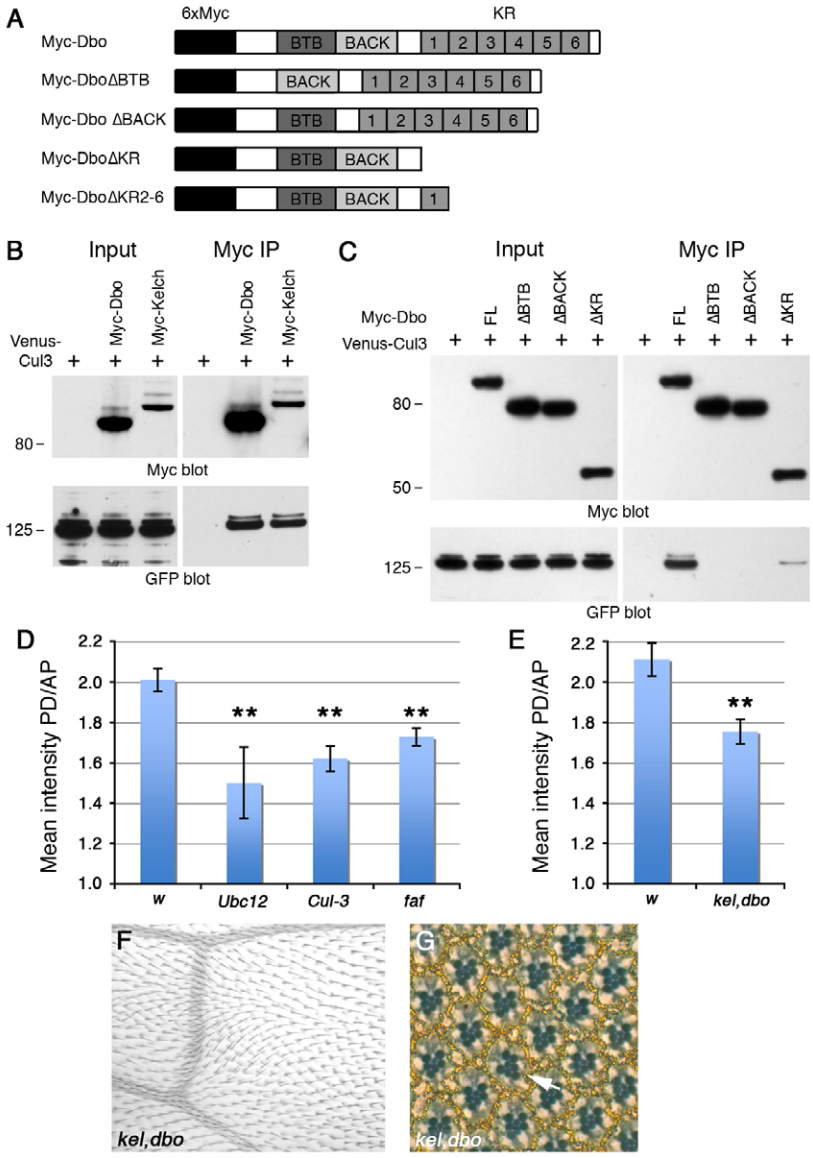

Fig. 3. Ubiquitylation regulates core protein asymmetry. (**A**) Myc-Dbo, showing the position of the BTB and BACK domains and the Kelch repeats (KR). Beneath are the deletion constructs used in the pulldown experiments. (**B**,**C**) Western blots showing pulldown of Venus-Cul-3 by Myc-tagged Dbo and Kelch (B) and the full-length (FL) and deleted forms of Myc-Dbo (C). Loading of input is 10% of pulldown. Molecular mass (kDa) is shown to the left. Anti-GFP recognises Venus-Cul-3. DboΔBTB and DboΔBTB no longer bind to Cul-3, whereas DboΔKR still binds but only weakly, suggesting that deletion of the Kelch repeats might perturb the secondary structure of the BTB/BACK domains. (**D**,**E**) Mean intensity of Fmi staining on proximodistal (PD) junctions (>45° from horizontal) relative to anterior-posterior (AP) junctions (<45° from horizontal) in wings expressing $w^{IR\text{-}30033}$, $Ubc12^{IR\text{-}7375R\text{-}3}$, $Cul\text{-}3^{IR\text{-}109415}$ and $faf^{IR\text{-}2956}$ using *MS1096-GAL4* (D) or in wings from w^{1118} and $kel^{DE1}; dbo^{\Delta 25.1}$ double-mutant flies (E). Asymmetry was scored below vein 4 (see supplementary material Fig. S3A-G). As *MS1096-GAL4* is more strongly expressed dorsally, asymmetry in these wings was scored on the dorsal surface only. Error bars indicate s.e.m.; $^{**}P<0.01$. (**F**,**G**) $kel^{DE1}; dbo^{\Delta 25.1}$ double-mutant wing (F) and adult eye section (G). Trichome swirls are only seen below vein 4, and ~1% of ommatidia are mispolarised. Arrow points to a mispolarised ommatidium.

(Fig. 3G). Knockdown of *Ubc12* and *Cul-3* caused pleiotropic effects, preventing analysis of trichome polarity defects. However, expression of *Ubc12* RNAi using *ptc-GAL4* caused trichomes to point towards the *ptc-GAL4* domain (supplementary material Fig. S3K), indicative of misoriented cell polarity.

Neddylation and ubiquitylation pathways target Dsh and Fmi

Abnormal ubiquitylation causes an increase or decrease of all the core proteins at junctions. The most probable scenario is that one core protein is the target of the ubiquitylation or deubiquitylation pathways and altered levels of this protein drive a similar alteration in the others. Likely targets of Dbo/Kel are the cytoplasmic proteins Dsh, Pk and Dgo, as their overexpression is known to cause accumulation of all the other core proteins at junctions (Feiguin et al., 2001; Tree et al., 2002; Bastock et al., 2003). Furthermore, in vertebrate canonical Wnt signalling, Dsh levels are regulated by a Cul-3-BTB E3 ubiquitin ligase complex (Angers et al., 2006), making Dsh a plausible substrate of a similar complex in planar polarity signalling in *Drosophila*.

Notably, loss of *pk* or *dgo* activity did not affect the ability of *Ubc12* or *Cul-3* RNAi to cause an accumulation of core proteins at junctions (compare supplementary material Fig. S4C,D and S4G,H with Fig. 2A and Fig. 1G, respectively; supplementary material Table S5). However, the increase in core protein levels at junctions was suppressed when dsh^{V26} clones were induced in wings expressing either *Ubc12* or *Cul-3* RNAi (Fig. 4A,B), or in $dsh^{V26}; kel^{DE1}$ double-mutant clones (Fig. 4C). Fz and Stbm are required for normal recruitment of Dsh to the plasma membrane (Axelrod, 2001; Shimada et al., 2001; Bastock et al., 2003). Loss of their activities also suppressed the effects of *Cul-3*, *Ubc12* and *kel; dbo* RNAi (supplementary material Fig. S4A,B,E,F,J,K, Table S5), again consistent with Dsh being the target.

Interestingly, whereas loss of *fz* and *dsh* completely suppressed the increase in core protein levels in wings expressing *Cul-3* RNAi (Fig. 4B; supplementary material Fig. S4A), there was still a residual increase in core protein levels in wings expressing *Ubc12* RNAi (supplementary material Fig. S4E,I). This suggests that Ubc12 might also affect core proteins by a second mechanism that is independent of Cul-3 and Dsh. For example, core proteins could

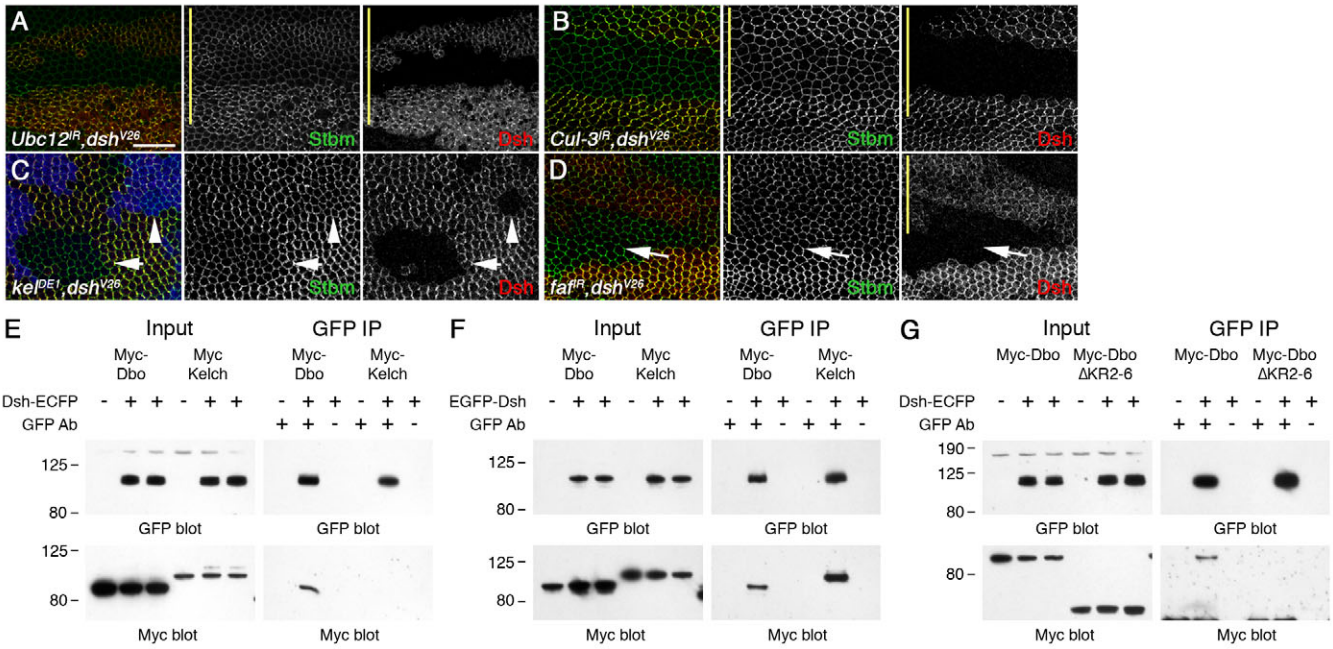

Fig. 4. Dsh is the target of Cul-3-Dbo/Kel. (**A-D**) *dsh*^{V26} *FRT19A/FRT19A; ptc-GAL4/+; Ubc12*$^{IR\text{-}7375R\text{-}3}$*, Ubx-FLP/+* (A), *dsh*^{V26} *FRT19A/Ubx-FLP FRT19A; ptc-GAL4/Cul-3*$^{IR\text{-}109415}$ (B), *dsh*^{V26} *FRT19A/Ubx-FLP FRT19A; kel*^{DE1} *FRT40/arm-lacZ FRT40* (C) and *dsh*^{V26} *FRT19A/Ubx-FLP FRT19A; ptc-GAL4/+; faf*$^{IR\text{-}2956}$*/+* (D). Wings are stained for Stbm (green), Dsh (red) and β-gal (blue, C); yellow bars mark the *ptc-GAL4* domain. Compare Stbm levels in the same wing in the presence or absence of *dsh* activity. (A,B) Stbm no longer accumulates in *dsh* clones. (C) In *dsh; kel* double-mutant tissue (arrow), Stbm no longer accumulates compared with *kel* mutant tissue (loss of blue), and levels are similar to those upon loss of *dsh* alone (arrowhead). (D) The *dsh* clone crosses the *ptc-GAL4* boundary, and where *faf*^{IR} is expressed (above the arrow) Stbm levels are decreased. Scale bar: 20 μm. (**E-G**) Western blots showing pulldown of Myc-tagged Dbo and Kelch by GFP-tagged Dsh in S2 cells (E,G) and COS-7 cells (F). Loading of input is 1% of pulldown. Molecular mass (kDa) is shown to the left.

be regulated via another Cullin homologue, or by direct neddylation of core proteins (Jones et al., 2008).

By contrast, loss of *dsh* activity did not alter the reduction of core protein levels caused by *faf* RNAi, indicating that Dsh is not the target of Faf (Fig. 4D; supplementary material Table S5). Likewise, core protein levels were still reduced when *faf* RNAi was expressed in *fz*, *stbm*, *pk* or *dgo* mutant backgrounds (supplementary material Fig. S4L-O, Table S5). Therefore, Faf is acting upstream of the other core proteins, consistent with it acting at the level of Fmi itself, either targeting Fmi directly or acting via an unknown adaptor protein. Note that because Fmi is normally required to recruit all of the other core proteins to junctions (Feiguin et al., 2001; Shimada et al., 2001; Strutt, 2001; Tree et al., 2002; Bastock et al., 2003), we were unable to directly determine whether Fmi is required for the effect of *faf* knockdown on the other core proteins.

The effects of Cul-3-Dbo/Kel and Faf on core protein levels could be mediated by direct regulation of Dsh and Fmi protein levels or via transcriptional regulation. Tagged forms of Dsh and Fmi expressed under ubiquitous promoters also increased or decreased when *Cul-3* or *faf* RNAi was expressed, suggesting that their effect is post-transcriptional (supplementary material Fig. S5A,B).

To test whether Dsh could be a direct target of Dbo/Kel, we expressed tagged Dsh and Dbo or Kel in S2 cells, and found that Dbo co-immunoprecipitated with Dsh (Fig. 4E), although only poorly, suggesting a weak or transient interaction. BTB domain proteins bind their substrates via the Kelch repeats (Petroski and Deshaies, 2005), and, consistent with the Dbo-Dsh interaction being specific, Dbo lacking all but one of its Kelch repeats no longer binds Dsh (Fig. 4G). Kel was not pulled down with Dsh in S2 cells, possibly owing to its poor expression (Fig. 4E), but both Dbo and Kel were pulled down with Dsh in COS-7 cells (Fig. 4F).

Ubiquitylation targets junctional Dsh for degradation

We next asked whether alterations in core protein levels at junctions reflect a change in the total cellular amount of protein or whether the ubiquitylation machinery acts specifically on a junctional population. Interestingly, although Dsh levels at junctions were increased several fold when *Ubc12* or *Cul-3* RNAi was expressed throughout the wing (see quantitation in supplementary material Fig. S6A-C,H), western blotting revealed that overall Dsh levels did not change (Fig. 5A,B). Overall Dsh levels were also unaltered in *kel; dbo* double-mutant wings (Fig. 5C,D; see also supplementary material Fig. S6D,E,I). Thus, ubiquitylation specifically regulates Dsh levels at junctions.

We then investigated whether expression of Dbo is sufficient to alter Dsh levels *in vivo*. Expression of *UAS-Myc-dbo* using the *ptc-GAL4* driver caused strong trichome swirling in the adult wing (Fig. 5K) and a strong reduction in the levels of Dsh at junctions in pupal wings (Fig. 5I). Interestingly, expression of *UAS-Myc-dbo* throughout the wing caused a significant decrease in total Dsh levels (Fig. 5E,F), consistent with Dbo not only redistributing Dsh from junctions to the cytoplasm but also targeting Dsh for degradation.

We then considered how the ubiquitylation machinery might recognise junctional Dsh. One possibility is that the Dbo/Kel E3 ligase subunits are localised to junctions; however, expression of Myc-Dbo at low levels revealed a diffuse localisation, with only a slight enrichment in plasma membrane puncta that do not colocalise

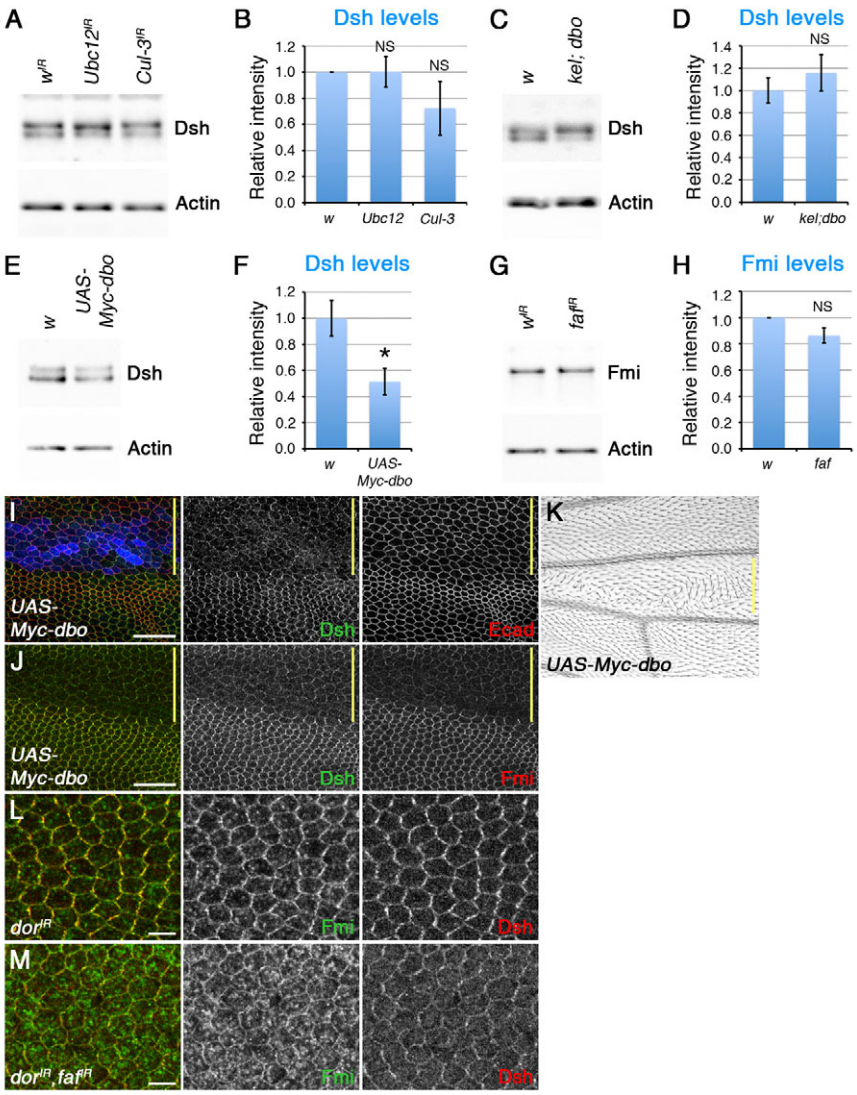

Fig. 5. Ubiquitylation targets junctional Dsh and Fmi for degradation. (**A-H**) Western blots probed for Dsh (A,C,E) or Fmi (G) and Actin (A,C,E,G) and quantitation of Dsh (B,D,F) and Fmi (H) levels, normalised to Actin loading control. Extracts are from male pupal wings expressing $w^{IR\text{-}30033}$, $Ubc12^{IR\text{-}7375R\text{-}3}$, $Cul\text{-}3^{IR\text{-}109415}$, $faf^{IR\text{-}2956}$ or *UAS-Myc-dbo* with *MS1096-GAL4* (A,E,G), or from w^{1118} or *kel; dbo* pupal wings (C). The Dsh blot shows two bands, which correspond to hyperphosphorylated and unphosphorylated forms of Dsh (Yanagawa et al., 1995). Quantitation is from western blots of three biological replicates. Error bars indicate s.e.m.; NS, not significant; *P=0.02. (**I-K**) *ptc-GAL4, UAS-Myc-dbo* adult wing (K) or pupal wings (I,J) stained for Dsh (green), Ecad (red in I), Fmi (red in J) and Myc (blue in I). Yellow bars mark the *ptc-GAL4* domain. (**L**,**M**) $dor^{IR\text{-}33733}$*/w; ptc-GAL4/+* (L) or $dor^{IR\text{-}33733}$*/w; ptc-GAL4/+;* $faf^{IR\text{-}2956}$*/+* (M) pupal wings stained for Fmi (green) and Dsh (red). Images are within the *ptc-GAL4* domain. Scale bars: 20 µm in I,J; 5 µm in L,M.

with core proteins (supplementary material Fig. S7A). Instead, we think it more likely that junctional Dsh is marked for ubiquitylation by post-translational modification, as is frequently the case for substrates of Cullin E3 ligases (Petroski and Deshaies, 2005) (see Discussion).

Surprisingly, decreased Dsh at junctions was accompanied by a reduction in Fmi levels (Fig. 5J), suggesting that when Dsh is removed from junctions by Dbo/Kel it can also promote, either directly or indirectly, the internalisation of Fmi. This is in line with previous observations that Fmi levels increase in a *dsh* mutant background (Shimada et al., 2001; Strutt and Strutt, 2008). One possibility is that Dsh acts as an endocytic adaptor for Fmi; however, we were unable to detect any colocalisation of Fmi and Dsh in intracellular vesicles (supplementary material Fig. S7B,C), implying that any association between them during Fmi internalisation would be transient (see Discussion). Blocking lysosomal maturation with mutations in *deep orange* (*dor*) results in intracellular accumulation of Fmi (Strutt and Strutt, 2008), consistent with some population of Fmi normally being sent to the lysosome for degradation. Knockdown of *dor* did not however cause any accumulation of Dsh (supplementary material Fig. S7D), suggesting that Dsh is not degraded in the lysosome, and must instead be proteasomally degraded.

Loss of Faf increases lysosomal degradation of Fmi

We next investigated whether overall Fmi levels are altered in wings expressing *faf* RNAi. Again, overall Fmi levels showed negligible change even though Fmi levels at junctions were substantially decreased (Fig. 5G,H; supplementary material Fig. S6F,G,J), suggesting that only the junctional population of Fmi is susceptible to regulation by the ubiquitylation machinery. The simplest model is that Fmi is targeted for internalisation by ubiquitylation, and that the deubiquitylating activity of Faf allows Fmi to return to the plasma membrane. Importantly, simultaneous knockdown of *faf* and *dor* causes more extensive accumulation of Fmi in intracellular vesicles than knockdown of *dor* alone (Fig. 5L,M), consistent with a failure of Fmi deubiquitylation normally promoting lysosomal degradation of Fmi.

We also investigated whether Faf localises with Fmi on endosomes. EGFP-tagged Faf showed a diffuse cytoplasmic distribution and we were unable to see any colocalisation with Fmi (supplementary material Fig. S7E,F).

Ubiquitylation of Dsh by Cul-3-Dbo/Kel does not modulate canonical Wingless signalling

In vertebrate embryos, loss of the Dbo/Kel-related protein KLHL12 increases canonical Wingless (Wg) signalling, presumably by

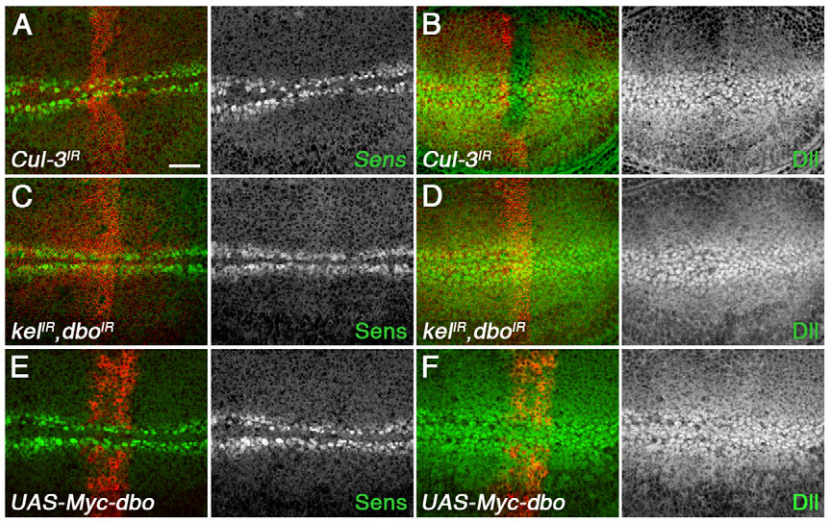

Fig. 6. Cul-3, Dbo and Kel do not regulate canonical Wg signalling. (**A-F**) *ptc-GAL4/Cul-3*$^{IR\text{-}109415}$ (A,B), *ptc-GAL4/dbo*$^{IR\text{-}105407}$*; kel*$^{IR\text{-}JF01768}$*/UAS-Dcr2* (C,D) and *ptc-GAL4/UAS-Myc-dbo* (E,F) wing discs, stained for Sens (green or white in A,C,E) or Dll (green or white in B,D,F). *ptc-GAL4* domain is marked by Fmi (red in A-D) or Myc (red in E,F). Note that *Cul-3*^{IR} wing discs are distorted, so Fmi staining is uneven. Wg signalling promotes Sens and Dll expression, and is unaltered. Scale bar: 20 μm.

stabilising Dsh (Angers et al., 2006). By contrast, reduced ubiquitylation did not increase overall levels of Dsh in fly wings (Fig. 5A-D). Consistent with this, we also saw no ectopic Wg signalling in wing discs expressing *Cul-3* or *kel; dbo* RNAi (Fig. 6A-D). Furthermore, there was no reduction in Wg signalling when Dbo was overexpressed (Fig. 6E,F), despite the striking effect on Dsh levels at junctions (Fig. 5I,J) and the reduction in overall Dsh levels (Fig. 5E,F).

DISCUSSION

In this study we have identified two ubiquitylation pathways that control the levels of planar polarity proteins at junctions, acting at the level of Dsh and Fmi. Mutations in ubiquitylation pathway components show that both increased and decreased levels of core proteins at junctions result in decreased asymmetry, suggesting that protein levels must be finely tuned in order for asymmetric localisation to be maximised.

With regard to adult planar polarity patterning, the decrease in asymmetry we observed does not lead to severe phenotypes in the wing and eye (Fig. 3F,G). However, it is well established that both tissues have downstream amplifiers to ensure a clearly polarised outcome, as correct polarisation can be achieved with little or no visible core protein asymmetry (Strutt and Strutt, 2007). However, in more dynamic contexts in which such downstream amplifiers might not exist or have time to act, such a reduction of core protein asymmetry would be expected to have severe effects on the final polarity of the tissue.

It is widely accepted that core protein polarity is produced by amplification of a weak initial cue by feedback loops. Such feedback loops could be caused by positive protein interactions, which promote the local accumulation of core proteins of the same species, or by negative interactions that inhibit their accumulation. The actual contribution of positive- or negative-feedback interactions is currently unknown, although mechanisms for both have been proposed (Tree et al., 2002; Jenny et al., 2005; Strutt et al., 2011). In practice, both are likely to operate, as amplification by positive interactions alone might lead to an uninhibited spread of polarised domains (Gierer and Meinhardt, 1972). Notably, one of the simplest forms of negative-feedback interaction is to limit the supply of substrate and we propose that this is the role of the pathways that we have characterised here.

Our observations can be simply explained in the light of such models. If an amplification system operates for local clustering of polarised core protein complexes [as we previously proposed (Strutt et al., 2011)], then the presence of excess core proteins in the junctions will lead to the excess growth of polarised domains and a possible reduction in the degree of overall cellular asymmetry. Conversely, a reduced level of core proteins will result in less efficient clustering of polarised protein complexes (as proteins of the same species would meet less often), again leading to a reduction in cellular asymmetry (Fig. 7A).

The cytoplasmic core proteins (Dsh, Pk and Dgo) appear to be of particular importance in the clustering of asymmetric complexes (Strutt et al., 2011), and overexpression of any of them appears to cause excessive clustering (Feiguin et al., 2001; Tree et al., 2002; Bastock et al., 2003). Our data suggest that Dsh is a direct target of a Cul-3-Dbo/Kel ubiquitin ligase complex, and the ubiquitylation and consequent removal of Dsh from junctions is thus a mechanism by which local Dsh levels are regulated.

Interestingly, in ubiquitylation pathway mutants, total cellular levels of Dsh are unaltered, even though levels at apical junctions increase several fold. This suggests that, in this context, ubiquitylation is a specific regulatory event at junctions. We do not know how the ubiquitylation machinery recognises junctional Dsh. One attractive possibility is that phosphorylated Dsh is the target for the Dbo/Kel E3 ligase. Phosphorylation is commonly used as a signal for the recruitment of ubiquitin ligases to their substrates (Petroski and Deshaies, 2005), and Dsh recruitment to junctions correlates with its hyperphosphorylation (Axelrod, 2001; Shimada et al., 2001). Interestingly, in *kel; dbo* double-mutant wings there is a small but significant increase in the upper, hyperphosphorylated Dsh band at the expense of the lower, unphosphorylated form (Fig. 5C; supplementary material Fig. S6K). Thus, loss of ubiquitylation could lead to an excessive accumulation of hyperphosphorylated Dsh at junctions, consistent with the proposal that ubiquitylation pathways normally act to remove hyperphosphorylated Dsh.

We note that ubiquitylation apparently does not act to remove the total population of hyperphosphorylated junctional Dsh, and so we speculate that either all of the Dsh at junctions is not phosphorylated on the relevant sites to trigger ubiquitylation, or that some of the hyperphosphorylated population of Dsh is protected. Biochemical analyses to directly show that hyperphosphorylated Dsh is specifically ubiquitylated have not proved feasible given the difficulty of obtaining large quantities of tissue of the relevant stage and the small proportion of cellular Dsh that is likely to be modified

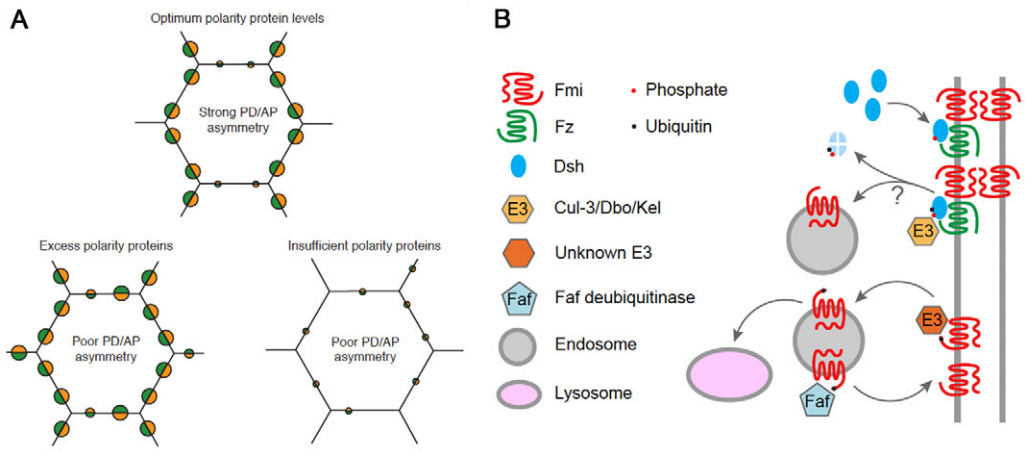

Fig. 7. Models for regulation of core protein levels at junctions by ubiquitylation. (**A**) Regulation of asymmetry by core protein levels. Green/orange semicircles represent plasma membrane puncta of asymmetrically localised Fz/Stbm complexes. Proximal is to the left and distal to the right. Under normal conditions, feedback loops ensure that Fz is mostly distal, and Stbm is mostly proximal within each cell. An excess of core proteins at junctions driven by loss of Dsh ubiquitylation leads to suboptimal feedback amplification, such that the domain of polarised complexes spreads too far around the cell periphery. Conversely, too little Fmi at junctions results in asymmetric molecular complexes failing to meet and therefore either clustering (feedback caused by positive protein interactions) or mutual inhibition (feedback caused by negative interactions) is abrogated. (**B**) Regulation of Dsh and Fmi levels by Dbo/Kel and Faf. Dsh is recruited to junctions by Fz and phosphorylated, and this correlates with clustering of asymmetric complexes of the same orientation. Dbo/Kel recognises junctional Dsh, and ubiquitylates excess Dsh leading to its removal from junctions and degradation, most likely by the proteasome (pale blue). Removal of Dsh from junctions also leads to endocytosis of Fmi. An unknown E3 ligase also promotes Fmi internalisation and lysosomal targeting, either by direct ubiquitylation of Fmi (as shown) or of an adaptor protein. Faf normally deubiquitylates some proportion of this internalised Fmi (or a Fmi adaptor) and allows Fmi to be recycled to the plasma membrane.

at any particular time. Similarly, experiments in cell lines are problematic as there is no suitable system for generating a polarised junctional population of *Drosophila* Dsh in culture, and again the relevant proportion of the total cellular population of Dsh would be very small.

It has been reported previously that, in *dsh* mutant clones, Fmi levels, but not Fz levels, increase (Shimada et al., 2001; Strutt and Strutt, 2008). This is indicative of a role for Dsh in removing some population of Fmi from junctions, possibly one that is not stably incorporated into asymmetric complexes. We now present further evidence for this role of Dsh, as overexpression of Myc-Dbo causes not only removal of the junctional population of Dsh but also the removal of Fmi. It remains to be determined whether Dsh co-traffics with Fmi, and whether this is the normal mode of removal of Dsh from junctions; however, it is interesting to note that in vertebrates Dsh has been reported to act as an endocytic adapter (Chen et al., 2003; Yu et al., 2007), and in some contexts such adaptors are marked for internalisation by ubiquitylation (reviewed by Traub and Lukacs, 2007). Nevertheless, we were unable to detect colocalisation of Fmi and Dsh in intracellular vesicles, suggesting that if Dsh does act as an adaptor for Fmi and is internalised with it, then Dsh must rapidly dissociate from Fmi before Fmi enters sorting endosomes. Interestingly, if this were the case, then Fmi (or another associated protein) would also have to be ubiquitylated if Fmi were to be subsequently targeted to the lysosome (Clague et al., 2012).

Fmi is known to accumulate in late endosomes when lysosomal targeting is blocked (Strutt and Strutt, 2008), consistent with it being internalised by a ubiquitin-dependent mechanism. Here, we identify the deubiquitylating enzyme Faf as a key regulator of junctional levels of Fmi. Furthermore, we show that loss of *faf* enhances the intracellular accumulation of Fmi when lysosomal targeting is blocked, suggesting that failure to deubiquitylate Fmi (or an adaptor) causes excess degradation of Fmi. As Fmi levels at junctions decrease in *faf* mutants, this suggests that recycling of Fmi is essential to maintain sufficient Fmi at junctions. However, we do not know whether Fmi is a direct ubiquitylation target as we were unable to co-immunoprecipitate Fmi and Faf in S2 cells due to their poor expression.

To summarise, we propose a model in which protein levels at junctions are regulated at multiple levels (Fig. 7B). Junctional, phosphorylated Dsh promotes clustering of asymmetric complexes. The level of Dsh at junctions is regulated by Dbo/Kel so as to prevent excess clustering, with ubiquitylated Dsh being removed from junctions and targeted for proteasomal degradation. Dsh could also act as an adaptor in order to remove excess Fmi that is not in complexes from junctions. Fmi is itself also a direct or indirect target of ubiquitylation, and this leads to internalisation of Fmi and targeting of Fmi to the lysosome. Recycling of this population of Fmi to the plasma membrane is promoted by activity of the deubiquitinase Faf.

Interestingly, in vertebrates Dsh has also been reported to be a target of a Cul-3-BTB E3 ligase. However, loss of KLHL12, a vertebrate BTB-Kelch family protein, causes gain-of-function Wnt signalling defects but no planar polarity defects (Angers et al., 2006). Nevertheless, planar polarity defects are seen when KLHL12 is overexpressed, probably owing to excess degradation of Dsh. By contrast, we do not detect any gain-of-function Wnt signalling phenotypes following a reduction in Cul-3-Dbo/Kel activity in flies, consistent with the unaltered total cellular levels of Dsh. Furthermore, even though total Dsh levels are significantly reduced when Dbo is overexpressed, this again does not noticeably affect Wnt signalling, suggesting that the remaining Dsh is sufficient for Wnt signalling activity. This suggests that the Cul-3-Kel/Dbo ubiquitylation mechanism plays a specific role in planar polarity in flies.

Acknowledgements
We thank the Bellen, Carroll, Chien, Fischer, Hong and Skeath labs, The Bloomington Stock Center, Developmental Studies Hybridoma Bank (DSHB), BioServ UK, Vienna Drosophila RNAi Center (VDRC), National Institute of

Genetics (NIG) and Drosophila RNAi Screening Center (DRSC) for fly stocks, antibodies and vectors.

Funding
This work was supported by a Wellcome Trust Senior Fellowship to D.S. and the Medical Research Council (MRC). Confocal facilities were provided by the Wellcome Trust and Yorkshire Cancer Research. Deposited in PMC for immediate release.

Competing interests statement
The authors declare no competing financial interests.

Supplementary material
Supplementary material available online at
http://dev.biologists.org/lookup/suppl/doi:10.1242/dev.089656/-/DC1

References

Aigouy, B., Farhadifar, R., Staple, D. B., Sagner, A., Röper, J.-C., Jülicher, F. and Eaton, S. (2010). Cell flow reorients the axis of planar polarity in the wing epithelium of Drosophila. *Cell* **142**, 773-786.
Amonlirdviman, K., Khare, N. A., Tree, D. R. P., Chen, W.-S., Axelrod, J. D. and Tomlin, C. J. (2005). Mathematical modeling of planar cell polarity to understand domineering nonautonomy. *Science* **307**, 423-426.
Angers, S., Thorpe, C. J., Biechele, T. L., Goldenberg, S. J., Zheng, N., MacCoss, M. J. and Moon, R. T. (2006). The KLHL12-Cullin-3 ubiquitin ligase negatively regulates the Wnt-beta-catenin pathway by targeting Dishevelled for degradation. *Nat. Cell Biol.* **8**, 348-357.
Axelrod, J. D. (2001). Unipolar membrane association of Dishevelled mediates Frizzled planar cell polarity signaling. *Genes Dev.* **15**, 1182-1187.
Bastock, R. and Strutt, D. (2007). The planar polarity pathway promotes coordinated cell migration during Drosophila oogenesis. *Development* **134**, 3055-3064.
Bastock, R., Strutt, H. and Strutt, D. (2003). Strabismus is asymmetrically localised and binds to Prickle and Dishevelled during Drosophila planar polarity patterning. *Development* **130**, 3007-3014.
Chen, X., Zhang, B. and Fischer, J. A. (2002). A specific protein substrate for a deubiquitinating enzyme: Liquid facets is the substrate of Fat facets. *Genes Dev.* **16**, 289-294.
Chen, W., ten Berge, D., Brown, J., Ahn, S., Hu, L. A., Miller, W. E., Caron, M. G., Barak, L. S., Nusse, R. and Lefkowitz, R. J. (2003). Dishevelled 2 recruits beta-arrestin 2 to mediate Wnt5A-stimulated endocytosis of Frizzled 4. *Science* **301**, 1391-1394.
Clague, M. J., Coulson, J. M. and Urbé, S. (2012). Cellular functions of the DUBs. *J. Cell Sci.* **125**, 277-286.
Classen, A. K., Anderson, K. I., Marois, E. and Eaton, S. (2005). Hexagonal packing of Drosophila wing epithelial cells by the planar cell polarity pathway. *Dev. Cell* **9**, 805-817.
Feiguin, F., Hannus, M., Mlodzik, M. and Eaton, S. (2001). The ankyrin repeat protein Diego mediates Frizzled-dependent planar polarization. *Dev. Cell* **1**, 93-101.
Gierer, A. and Meinhardt, H. (1972). A theory of biological pattern formation. *Kybernetik* **12**, 30-39.
Goodrich, L. V. and Strutt, D. (2011). Principles of planar polarity in animal development. *Development* **138**, 1877-1892.
Gray, R. S., Roszko, I. and Solnica-Krezel, L. (2011). Planar cell polarity: coordinating morphogenetic cell behaviors with embryonic polarity. *Dev. Cell* **21**, 120-133.
Hershko, A. and Ciechanover, A. (1998). The ubiquitin system. *Annu. Rev. Biochem.* **67**, 425-479.
Huang, Y., Baker, R. T. and Fischer-Vize, J. A. (1995). Control of cell fate by a deubiquitinating enzyme encoded by the fat facets gene. *Science* **270**, 1828-1831.
Huang, J., Zhou, W., Watson, A. M., Jan, Y. N. and Hong, Y. (2008). Efficient ends-out gene targeting in Drosophila. *Genetics* **180**, 703-707.
Hudson, A. M. and Cooley, L. (2010). Drosophila Kelch functions with Cullin-3 to organize the ring canal actin cytoskeleton. *J. Cell Biol.* **188**, 29-37.
Jenny, A., Reynolds-Kenneally, J., Das, G., Burnett, M. and Mlodzik, M. (2005). Diego and Prickle regulate Frizzled planar cell polarity signalling by competing for Dishevelled binding. *Nat. Cell Biol.* **7**, 691-697.
Jones, J., Wu, K., Yang, Y., Guerrero, C., Nillegoda, N., Pan, Z. Q. and Huang, L. (2008). A targeted proteomic analysis of the ubiquitin-like modifier nedd8 and associated proteins. *J. Proteome Res.* **7**, 1274-1287.
Le Garrec, J. F., Lopez, P. and Kerszberg, M. (2006). Establishment and maintenance of planar epithelial cell polarity by asymmetric cadherin bridges: a computer model. *Dev. Dyn.* **235**, 235-246.
McNeill, H. (2010). Planar cell polarity: keeping hairs straight is not so simple. *Cold Spring Harb. Perspect. Biol.* **2**, a003376.
Meinhardt, H. (2007). Computational modelling of epithelial patterning. *Curr. Opin. Genet. Dev.* **17**, 272-280.
Michelle, C., Vourc'h, P., Mignon, L. and Andres, C. R. (2009). What was the set of ubiquitin and ubiquitin-like conjugating enzymes in the eukaryote common ancestor? *J. Mol. Evol.* **68**, 616-628.
Mukai, A., Yamamoto-Hino, M., Awano, W., Watanabe, W., Komada, M. and Goto, S. (2010). Balanced ubiquitylation and deubiquitylation of Frizzled regulate cellular responsiveness to Wg/Wnt. *EMBO J.* **29**, 2114-2125.
Narimatsu, M., Bose, R., Pye, M., Zhang, L., Miller, B., Ching, P., Sakuma, R., Luga, V., Roncari, L., Attisano, L. et al. (2009). Regulation of planar cell polarity by Smurf ubiquitin ligases. *Cell* **137**, 295-307.
Ni, J. Q., Zhou, R., Czech, B., Liu, L. P., Holderbaum, L., Yang-Zhou, D., Shim, H. S., Tao, R., Handler, D., Karpowicz, P. et al. (2011). A genome-scale shRNA resource for transgenic RNAi in Drosophila. *Nat. Methods* **8**, 405-407.
Nolo, R., Abbott, L. A. and Bellen, H. J. (2000). Senseless, a Zn finger transcription factor, is necessary and sufficient for sensory organ development in Drosophila. *Cell* **102**, 349-362.
Oda, H., Uemura, T., Harada, Y., Iwai, Y. and Takeichi, M. (1994). A Drosophila homolog of cadherin associated with armadillo and essential for embryonic cell-cell adhesion. *Dev. Biol.* **165**, 716-726.
Overstreet, E., Fitch, E. and Fischer, J. A. (2004). Fat facets and Liquid facets promote Delta endocytosis and Delta signaling in the signaling cells. *Development* **131**, 5355-5366.
Panganiban, G., Sebring, A., Nagy, L. and Carroll, S. (1995). The development of crustacean limbs and the evolution of arthropods. *Science* **270**, 1363-1366.
Petroski, M. D. and Deshaies, R. J. (2005). Function and regulation of cullin-RING ubiquitin ligases. *Nat. Rev. Mol. Cell Biol.* **6**, 9-20.
Rabut, G. and Peter, M. (2008). Function and regulation of protein neddylation. 'Protein modifications: beyond the usual suspects' review series. *EMBO Rep.* **9**, 969-976.
Schüpbach, T. and Wieschaus, E. (1989). Female sterile mutations on the second chromosome of Drosophila melanogaster. I. Maternal effect mutations. *Genetics* **121**, 101-117.
Shimada, Y., Usui, T., Yanagawa, S., Takeichi, M. and Uemura, T. (2001). Asymmetric colocalization of Flamingo, a seven-pass transmembrane cadherin, and Dishevelled in planar cell polarization. *Curr. Biol.* **11**, 859-863.
Strutt, D. I. (2001). Asymmetric localization of frizzled and the establishment of cell polarity in the Drosophila wing. *Mol. Cell* **7**, 367-375.
Strutt, H. and Strutt, D. (2003). EGF signaling and ommatidial rotation in the Drosophila eye. *Curr. Biol.* **13**, 1451-1457.
Strutt, D. and Strutt, H. (2007). Differential activities of the core planar polarity proteins during Drosophila wing patterning. *Dev. Biol.* **302**, 181-194.
Strutt, H. and Strutt, D. (2008). Differential stability of flamingo protein complexes underlies the establishment of planar polarity. *Curr. Biol.* **18**, 1555-1564.
Strutt, H., Price, M. A. and Strutt, D. (2006). Planar polarity is positively regulated by casein kinase lepsilon in Drosophila. *Curr. Biol.* **16**, 1329-1336.
Strutt, H., Warrington, S. J. and Strutt, D. (2011). Dynamics of core planar polarity protein turnover and stable assembly into discrete membrane subdomains. *Dev. Cell* **20**, 511-525.
Tauriello, D. V., Haegebarth, A., Kuper, I., Edelmann, M. J., Henraat, M., Canninga-van Dijk, M. R., Kessler, B. M., Clevers, H. and Maurice, M. M. (2010). Loss of the tumor suppressor CYLD enhances Wnt/beta-catenin signaling through K63-linked ubiquitination of Dvl. *Mol. Cell* **37**, 607-619.
Traub, L. M. and Lukacs, G. L. (2007). Decoding ubiquitin sorting signals for clathrin-dependent endocytosis by CLASPs. *J. Cell Sci.* **120**, 543-553.
Tree, D. R. P., Shulman, J. M., Rousset, R., Scott, M. P., Gubb, D. and Axelrod, J. D. (2002). Prickle mediates feedback amplification to generate asymmetric planar cell polarity signaling. *Cell* **109**, 371-381.
Usui, T., Shima, Y., Shimada, Y., Hirano, S., Burgess, R. W., Schwarz, T. L., Takeichi, M. and Uemura, T. (1999). Flamingo, a seven-pass transmembrane cadherin, regulates planar cell polarity under the control of Frizzled. *Cell* **98**, 585-595.
Vichas, A. and Zallen, J. A. (2011). Translating cell polarity into tissue elongation. *Semin. Cell Dev. Biol.* **22**, 858-864.
Wu, J. T., Lin, H. C., Hu, Y. C. and Chien, C. T. (2005). Neddylation and deneddylation regulate Cul1 and Cul3 protein accumulation. *Nat. Cell Biol.* **7**, 1014-1020.
Yanagawa, S.-i., van Leeuwen, F., Wodarz, A., Klingensmith, J. and Nusse, R. (1995). The dishevelled protein is modified by wingless signaling in Drosophila. *Genes Dev.* **9**, 1087-1097.
Yu, A., Rual, J. F., Tamai, K., Harada, Y., Vidal, M., He, X. and Kirchhausen, T. (2007). Association of Dishevelled with the clathrin AP-2 adaptor is required for Frizzled endocytosis and planar cell polarity signaling. *Dev. Cell* **12**, 129-141.

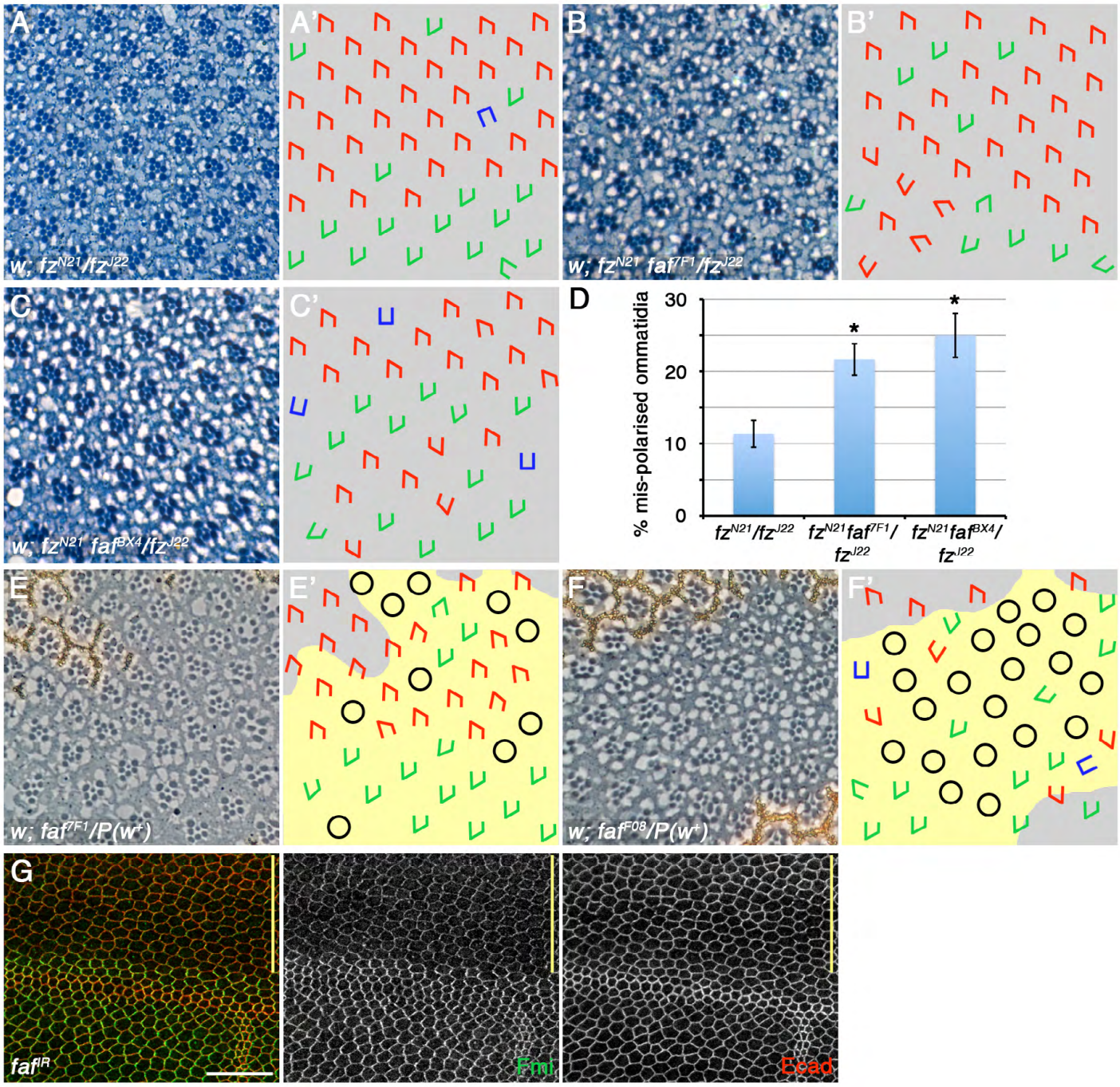

Fig. S1. *faf* mutant phenotypes. (**A-C′**) Adult eye sections and cartoons of fz^{N21}/fz^{J22} (A), fz^{N21} faf^{7F1}/fz^{J22} (B) and fz^{N21} faf^{BX4}/fz^{J22} (C). Red indicates dorsal ommatidia, green indicates ventral ommatidia and blue indicates achiral ommatidia. (**D**) The enhancement of the fz^{N21}/fz^{J22} ommatidial polarity phenotype by *faf*. Error bars are s.e.m.; *P<0.05. (**E-F′**) faf^{7F1} (E) and faf^{F08} (F) eye clones, marked by loss of white pigment, or yellow in the cartoons. Note that in *faf* mutant tissue many ommatidia have photoreceptor recruitment defects (black circles in cartoons), but in ommatidia with normal photoreceptor number there are frequent polarity defects, including chirality defects and misrotations. (**G**) *ptc-GAL4/+;* $faf^{IR\text{-}2956}$*/+* pupal wings stained for Fmi (green) or Ecad (red). Yellow bars mark the *ptc-GAL4* domain. Scale bar: 20 µm.

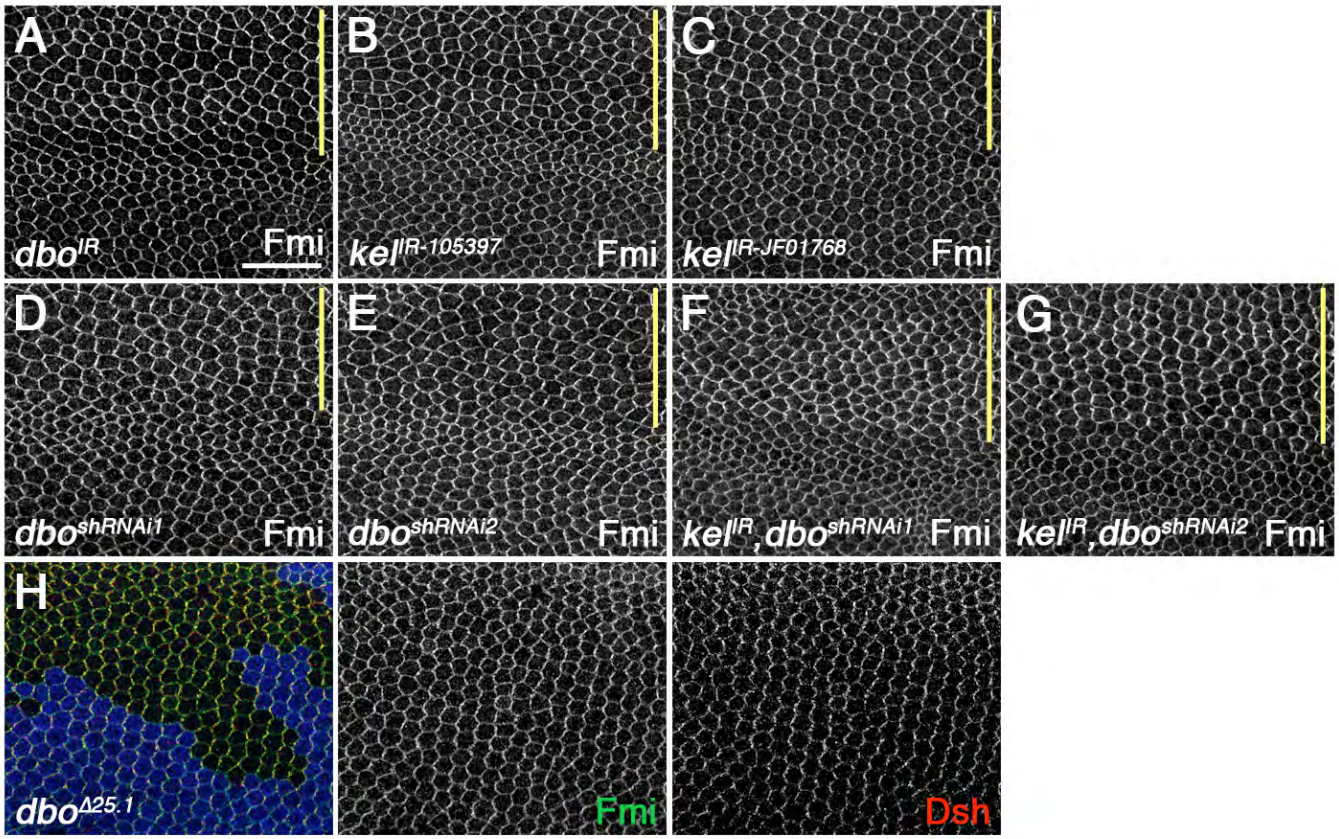

Fig. S2. Effects of RNAi against *dbo* and *kel*. (**A-G**) Pupal wings from *ptc-GAL4/dbo*$^{IR\text{-}105407}$*; UAS-Dcr2/+* (A), *ptc-GAL4/kel*$^{IR\text{-}105397}$*; UAS-Dcr2/+* (B), *ptc-GAL4/+; kel*$^{IR\text{-}JF01768}$*/UAS-Dcr2* (C), *ptc-GAL4/dbo*^{shRNAi1} (D), *ptc-GAL4/dbo*^{shRNAi2} (E), *ptc-GAL4/dbo*^{shRNAi1}*; kel*$^{IR\text{-}JF01768}$*/UAS-Dcr2* (F) and *ptc-GAL4/dbo*^{shRNAi2}*; kel*$^{IR\text{-}JF01768}$*/UAS-Dcr2* (G) stained for Fmi. Note that the increase in core protein localisation caused by RNAi against *dbo* and *kel* (A-C) was not apparent in every wing, probably owing to variations in staining and the flatness of the wings. (**H**) *dbo*$^{\Delta 25.1}$ pupal wing clone stained for Fmi (green) and Dsh (red); clone marked by loss of β-gal (blue). Yellow bars mark the *ptc-GAL4* domain. Scale bar: 20 µm.

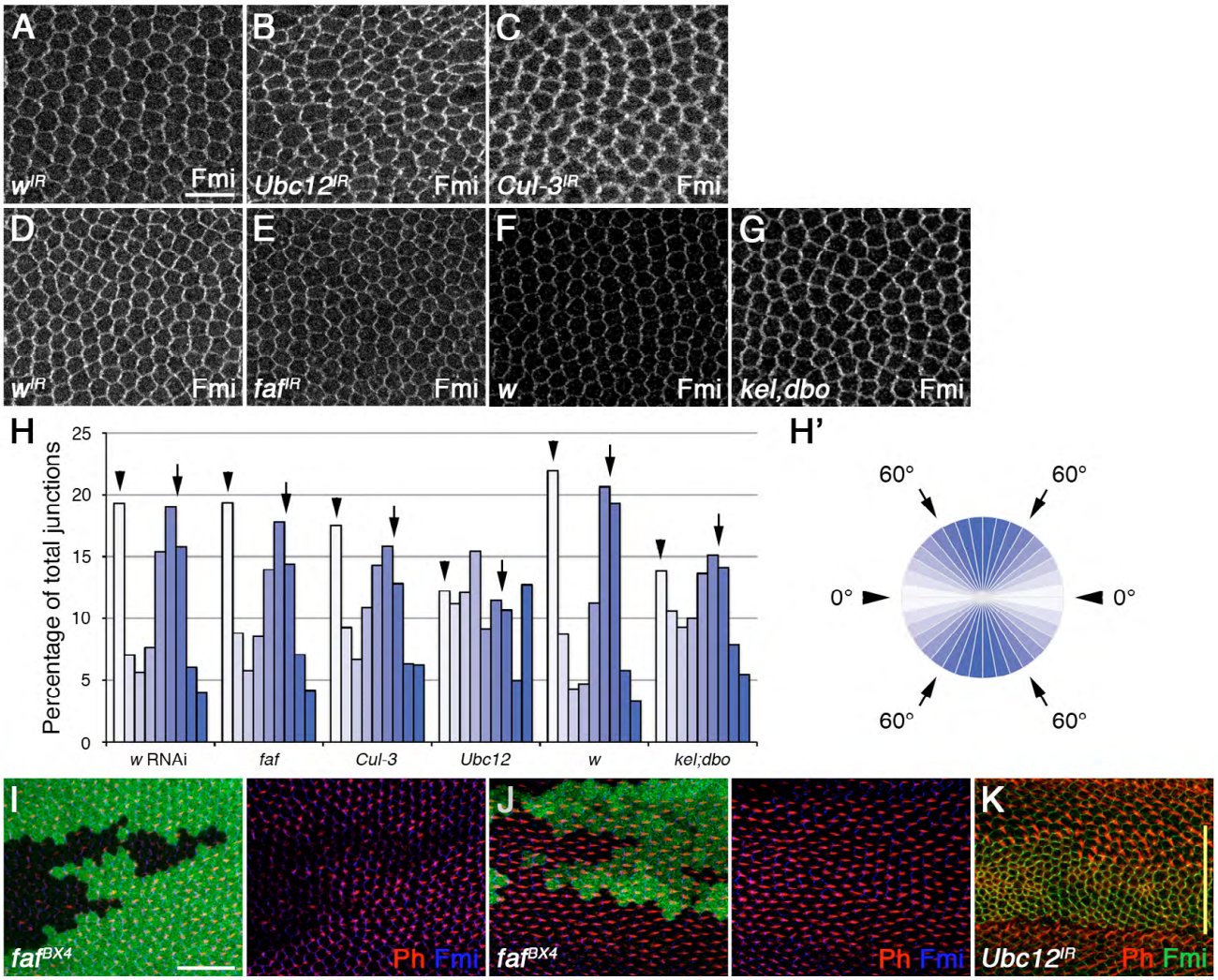

Fig. S3. Loss of asymmetry and trichome phenotypes of *Ubc12, Cul-3* and *faf*. (**A-E**) Male wings expressing $w^{IR\text{-}30033}$ (A,D), $Ubc12^{IR\text{-}7375R\text{-}3}$ (B), $Cul\text{-}3^{IR\text{-}109415}$ (C) and $faf^{IR\text{-}2956}$ (E) using *MS1096-GAL4*, stained with Fmi. (**F**,**G**) Pupal wings from w^{1118} (F) or kel^{DE1}; $dbo^{\Delta 25.1}$ double mutants (G), stained for Fmi. Sets of wings (A-C, D,E and F,G) were dissected, stained and imaged in parallel using the same confocal settings. All images are below vein 4. (**H**,**H′**) The percentage of junctions oriented at different angles, where 0° is horizontal and 90° is vertical, in the above genotypes. Angles are binned into 10° categories, where 0-10° is white and 80-90° is dark blue. The colour scheme of the differently oriented junctions is shown in H′. For a hexagonal array of cells, most junctions would be expected to be oriented at around 0° (arrowheads) or 60° (arrows). Cell packing is very irregular in wings expressing *Ubc12* RNAi, which appears to have pleiotropic effects. By contrast, cell packing is only mildly affected in *Cul-3*, *dbo; kel* and *faf* wings, in line with the known role of core proteins in regulating junctional rearrangement. (**I**,**J**) faf^{BX4} pupal wing clones stained for Fmi (blue) and with phalloidin (red); clones are marked by loss of β-gal (green), just after trichomes emerge in wild-type tissue (I) or when trichomes are slightly older (J). (**K**) *ptc-GAL4/+;* $Ubc12^{IR\text{-}7375R\text{-}3}$*/+* pupal wings stained for Fmi (green) and with phalloidin (red). Note trichomes are very delayed where high levels of *Ubc12* RNAi are expressed, and trichomes swirl towards the compartment boundary. Yellow bars mark the *ptc-GAL4* domain. Scale bars: 10 µm in A-G; 20 µm in I-K.

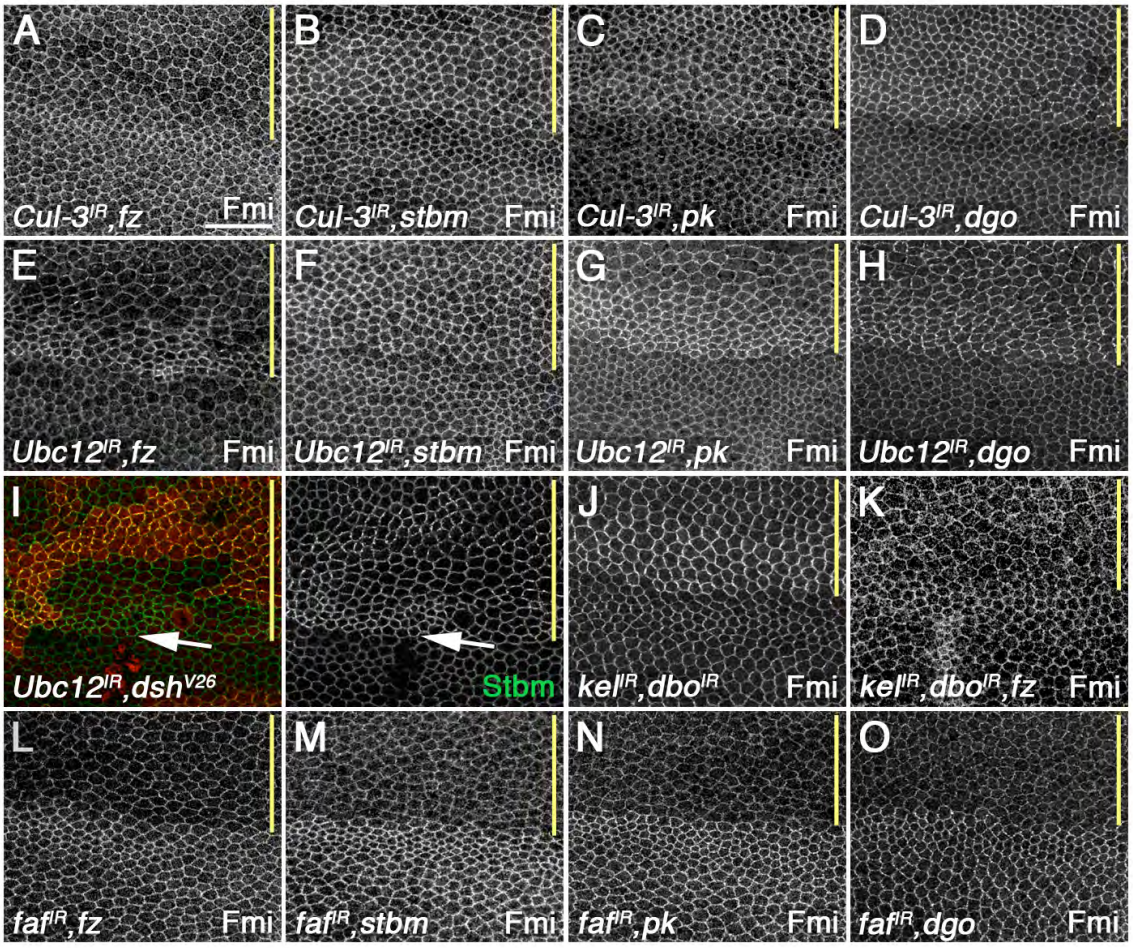

Fig. S4. Identification of the targets of Dbo/Kel and Faf. (**A-O**) *ptc-GAL4/Cul-3$^{IR\text{-}109415}$; fz^{P21}/fz^{P21}* (A), *ptc-GAL4, stbm^{6}/Cul-3$^{IR\text{-}109415}$, stbm^{6}* (B), *ptc-GAL4, pk$^{pk\text{-}sple13}$/Cul-3$^{IR\text{-}109415}$, pk$^{pk\text{-}sple13}$* (C), *ptc-GAL4, dgo^{380}/Cul-3$^{IR\text{-}109415}$, dgo^{380}* (D), *ptc-GAL4/+; Ubc12$^{IR\text{-}7375R\text{-}3}$, fz^{P21}/fz^{P21}* (E), *ptc-GAL4, stbm^{6}/stbm^{6}; Ubc12$^{IR\text{-}7375R\text{-}3}$/+* (F), *ptc-GAL4, pk$^{pk\text{-}sple13}$/pk$^{pk\text{-}sple13}$; Ubc12$^{IR\text{-}7375R\text{-}3}$/+* (G), *ptc-GAL4, dgo^{380}/dgo^{380}; Ubc12$^{IR\text{-}7375R\text{-}3}$/+* (H), *dsh^{V26} FRT19A/FRT19A; ptc-GAL4/+; Ubc12$^{IR\text{-}7375R\text{-}3}$, Ubx-FLP/+* (I), *ptc-GAL4/dbo$^{IR\text{-}105407}$; kel$^{IR\text{-}JF01768}$/+* (J), *ptc-GAL4/dbo$^{IR\text{-}105407}$; kel$^{IR\text{-}JF01768}$, fz^{P21}/fz^{P21}* (K), *ptc-GAL4/+; faf$^{IR\text{-}2956}$, fz^{P21}/fz^{P21}* (L), *ptc-GAL4, stbm^{6}/stbm^{6}; faf$^{IR\text{-}2956}$/+* (M), *ptc-GAL4, pk$^{pk\text{-}sple13}$/pk$^{pk\text{-}sple13}$; faf$^{IR\text{-}2956}$/+* (N) and *ptc-GAL4, dgo^{380}/dgo^{380}; faf$^{IR\text{-}2956}$/+* (O). Pupal wings are stained for Fmi, except for I which is stained for Stbm (green) and Dsh (red). Yellow bars mark the *ptc-GAL4* domain. Note that the *dsh* clone in I is very proximal in the wing and overlaps the AP compartment boundary, where *Ubc12* knockdown is strongest. *dsh* clones in more distal wing regions (where *Ubc12* knockdown is weaker) show complete suppression of the increase in core protein levels. In this proximal clone, *Ubc12* knockdown still induces a small increase in Stbm levels at junctions compared with wild-type tissue (below the arrow). Scale bar: 20 μm.

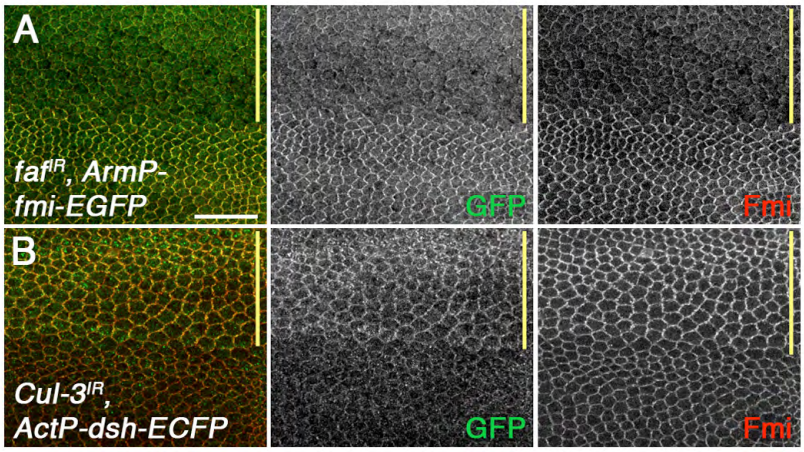

Fig. S5. Alteration of core protein levels is post-transcriptional. *ptc-GAL4/ArmP-Fmi-EGFP; faf$^{IR\text{-}2956}$/+* (**A**) and *Ubx-FLP; ptc-GAL4/Cul3$^{IR\text{-}109415}$; ActP-FRT-polyA-FRT-Dsh-ECFP/+* (**B**) pupal wings, stained for GFP (green) and Fmi (red). Yellow bars mark the *ptc-GAL4* domain. Scale bar: 20 μm.

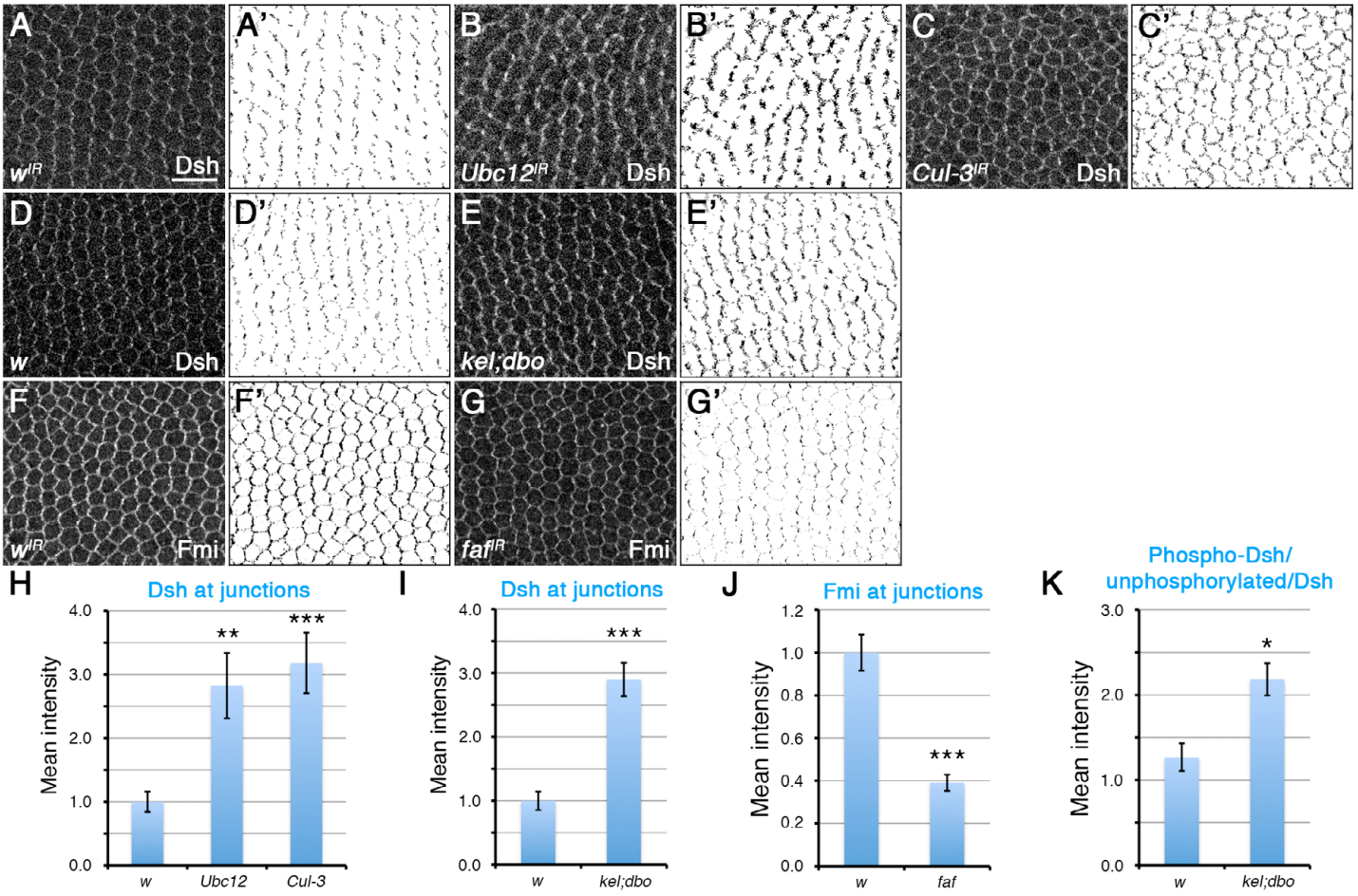

Fig. S6. Analysis of junctional levels of Dsh and Fmi. (**A-C**) Male pupal wings expressing $w^{IR\text{-}30033}$ (A), $Ubc12^{IR\text{-}7375R\text{-}3}$ (B) and $Cul\text{-}3^{IR\text{-}109415}$ (C) using *MS1096-GAL4*, stained for Dsh. (**D**,**E**) Pupal wings from w^{1118} and kel^{DE1}; $dbo^{\Delta 25.1}$ double mutants, stained for Dsh. (**F**,**G**) Male pupal wings expressing $w^{IR\text{-}30033}$ (F) and $faf^{IR\text{-}2956}$ (G) using *MS1096-GAL4*, stained for Fmi. Sets of wings (A-C, D,E and F,G) were dissected, stained and imaged in parallel using the same confocal settings. All images are below vein 4. Scale bar 10 µm. (**A′-G′**) Masks showing the area measured for intensity after thresholding the image (see Materials and methods). (**H-J**) Quantitation of junctional Dsh staining (H,I) or junctional Fmi staining (J) for the above genotypes. Error bars are s.e.m.; ***P<0.001, **P<0.01. (**K**) Quantitation of phosphorylated Dsh relative to unphosphorylated Dsh from western blots of w^{1118} and kel^{DE1}; $dbo^{\Delta 25.1}$ double mutants (see Fig. 5C). Quantitation is from western blots of three biological replicates. Error bars are s.e.m.; *P=0.02.

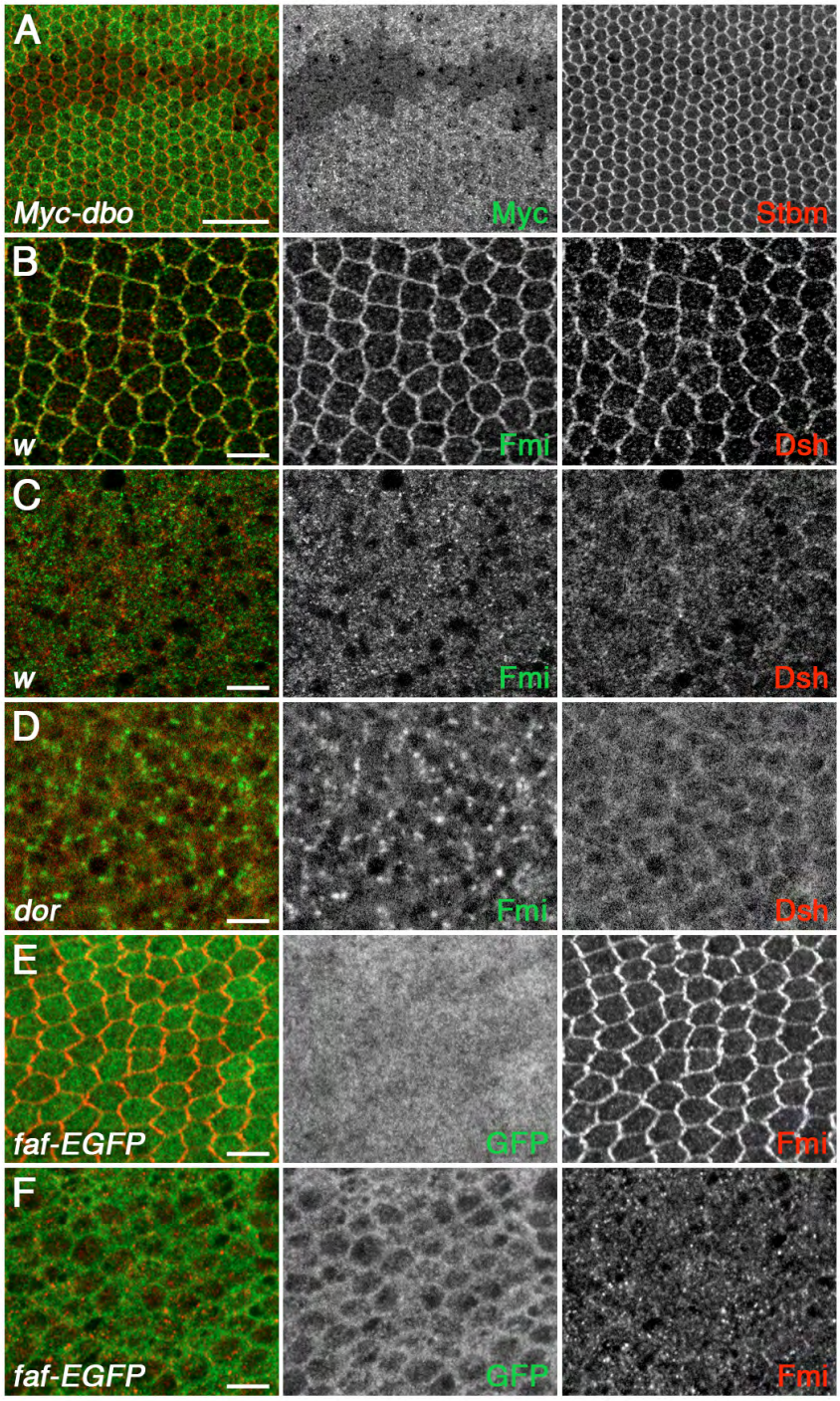

Fig. S7. Localisation of Dbo and Faf in pupal wings. (**A**) *Ubx-FLP; ActP-FRT-polyA-FRT-Myc-dbo/Δ2-3* pupal wings stained for Myc (green) and Stbm (red). (**B**,**C**) w^{1118} pupal wings stained for Fmi (green) and Dsh (red), with apical (B) and subapical (C) sections. (**D**) $dor^{JR\text{-}33733}$*/w; ptc-GAL4/+* pupal wings, stained for Fmi (green) and Dsh (red); subapical section (see Fig. 5L for junctional staining). Image is within the *ptc-GAL4* domain. (**E**,**F**) *Ubx-FLP; ActP-FRT-polyA-FRT-faf-EGFP/+* pupal wings stained for GFP (green) and Fmi (red), with apical (E) and subapical (F) staining. The *faf-EGFP* transgene rescues the *faf* mutant phenotype (not shown). Scale bars: 20 µm in A; 5 µm in B-F.

Table S1. Adult and pupal wing screen of genes encoding predicted E2 ubiquitin-conjugating enzymes

CG number	Gene symbol	RNAi line	*MS1096-GAL4* adult wing	*ptc-GAL4* pupal wing
CG10254	CG10254	GD 15992	wild type	wild type
		NIG 10254R-1	wild type	wild type
		NIG 10254R-2	wild type	wild type
		KK 108657	wild type	-
CG10536	*crbx*	GD 16078	wild type	wild type
		KK 101755	wild type	-
CG10640	*Uev1A*	GD 30890	variable hair orientation[#]	cell packing defect*
		GD 32267	variable hair orientation[#]	cell packing defect*
CG10682	*vih*	GD 27306	wild type	wild type
		KK 107720	vein defect	-
CG10862	CG10862	GD 31372	wild type	wild type
		GD 31373	variable hair orientation	wild type
		KK 101113	no polarity phenotype[‡]	wild type with narrow intervein
CG12799	*Ubc84D*	GD 20260	variable hair orientation	wild type
		NIG 12799R-2	variable hair orientation	-
		KK 106363	vein defect	-
CG14739	CG14739	GD 18358	wild type	wild type
		NIG 14739R-1	wild type	-
		NIG 14739R-2	wild type	-
		KK 105594	wild type	-
CG15437	CG15437	GD 11090	wild type	wild type
CG16894	CG16894	GD 10067	wild type	wild type
		GD 108983	wild type	-
CG17030	CG17030	GD 32827	variable hair orientation	wild type
		GD 32828	variable hair orientation	-
		NIG 17030R-1	variable hair orientation	-
		NIG 17031R-2	wild type	-
		KK 108804	wild type	-
CG18319	*ben*	GD 9413	wings disrupted	cell packing defect*
CG2013	CG2013	GD 23229	lethal	large, irregular cells
		GD 23230	lethal	large, irregular cells
		GD 46927	lethal	large, irregular cells
CG2257	CG2257	GD 33509	wings disrupted	cell packing defect*
		GD 33510	wings disrupted	cell packing defect*
CG2574	CG2574	GD 40173	wild type	wild type
		NIG 2574R-2	wild type	-
		NIG 2574R-3	wild type	-
		KK 105725	wild type	-
CG2924	CG2924	NIG 2924R-3	wild type	-
		KK 104482	wild type	-
CG3018	*lwr*	GD 33684	lethal	cell packing defect*
		GD 33685	lethal	cell packing defect*

CG number	Gene symbol	RNAi line	*MS1096-GAL4* adult wing	*ptc-GAL4* pupal wing
CG3473	CG3473	GD 26201	wild type	wild type
		NIG 3473R-2	wild type	-
		NIG 3473R-7	wild type	-
		KK 104207	no polarity phenotype‡	lethal
CG40045	CG40045	KK 109167	vein defect	-
CG4443	*crl*	GD 34109	variable hair orientation	wild type
		GD 34111	variable hair orientation	wild type
		NIG 4443R-1	variable hair orientation	-
		NIG 4443R-2	variable hair orientation	-
		KK 104440	wild type	-
CG4502	CG4502	GD 34855	wings disrupted	cell packing defect*
		GD 34858	wild type	wild type
CG5440	CG5440	GD 49029	wings disrupted	cell packing defect*
		GD 49030	-	wild type
		NIG 5440R-3	variable hair orientation	-
CG5788	CG5788	GD 27515	wings disrupted	cell packing defect*
		GD 48145	vein defect	cell packing defect*
		GD 48146	wings disrupted	cell packing defect*
CG5823	CG5823	GD 8301	wild type	wild type
		GD 33260	wild type	wild type
		NIG 5823R-1	wild type	-
		NIG 5823R-3	wild type	-
		KK 108292	wild type	-
CG6303	*Bruce*	NIG 6303R-1	wild type	-
		NIG 6303R-2	wild type	-
		KK 107620	ectopic bristles	-
CG6720	*UbcD2*	GD 31158	vein defect, possible swirls below vein 4	wild type
CG7220	CG7220	GD 34198	wild type	wild type
		GD 34199	wild type	wild type
		KK 104478	wild type	-
CG7375	*Ubc12*	GD 35219	wings disrupted	accumulation of Fmi
		GD 35220	wings disrupted	accumulation of Fmi
		NIG 7375R-2	wild type	wild type
		NIG 7375R-3	wings disrupted	accumulation of Fmi
		KK 100761	wings disrupted	accumulation of Fmi, cell morphology abnormal
CG7425	*eff*	GD 26011	late larval lethal	lethal
		NIG 7425R-1	wings disrupted	wild type
		NIG 7425R-2	wings disrupted	wild type
CG7656	CG7656	GD 26880	wild type	wild type
		GD 26881	variable hair orientation	cell packing defect*
		NIG 7656R-2	wild type	-
CG8188	CG8188	NIG 8188R-1	wild type	-
		NIG 8188R-2	wild type	-
		KK 103362	wings curly	wild type
CG8284	CG8284	GD 35872	wild type	wild type
		GD 35873	wild type	wild type
		KK 106600	ectopic bristles	-

CG number	Gene symbol	RNAi line	*MS1096-GAL4* adult wing	*ptc-GAL4* pupal wing
CG9602	CG9602	GD 29498	wild type	wild type
		GD 29499	vein defect	wild type
		NIG 9602R-2	wild type	-
		NIG 9602R-3	wild type	-

GD, GD collection of RNAi lines from VDRC.
KK, KK collection of RNAi lines from VDRC.
NIG, RNAi lines from NIG-FLY.
Wings disrupted: hair polarity could not be assessed as wings could not be mounted flat.
Cell packing defect: cells not organised in the normal hexagonal array.
Irregular cells: cell size and packing disturbed.
[#]Using ptc-GAL4.
[‡]Male wings not mountable, hinge defect in female wings.
*Fmi asymmetric in hexagonal cells.

Table S2. Adult and pupal wing screen of genes encoding neddylation pathway components

CG number	Gene symbol	RNAi line	*MS1096-GAL4* adult wing	*ptc-GAL4* pupal wing
CG10679	*Nedd8*	GD 28444	lethal	lethal
		GD 28445	lethal	lethal
CG13343	*Uba3*	GD 17137	wild type	wild type
		GD 17139	wild type	accumulation of Fmi
		NIG 13343R-4	wings disrupted	accumulation of Fmi
CG7828	*APP-BP1*	GD 7728	wild type	-
		NIG 7828R-2	wings slightly curly	-
		NIG 7828R-3	wild type	-
CG16982	*Roc1a*‡	GD 32399	lethal	accumulation of Fmi
CG16988	*Roc1b*‡	GD 32797	lethal	Cell packing defect, Fmi levels increase slightly?

GD, GD collection of RNAi lines from VDRC.
NIG, RNAi lines from NIG-FLY.
Wings disrupted: hair polarity could not be assessed as wings could not be mounted flat.
Cell packing defect: cells not organised in the normal hexagonal array.
‡Roc proteins are not specific to the neddylation pathway, as they are also subunits of Cullin E3 ligase complexes.

Table S3. Adult and pupal wing screen of genes encoding Cullins

CG number	Gene symbol	RNAi line	*MS1096-GAL4* adult wing	*ptc-GAL4* pupal wing
CG1877	*lin19/Cul-1*	GD 33406	lethal	wild type
		GD 33407	wild type	embryonic lethal 29°C
		GD 42445	lethal	pupal lethal 18°C
CG1512	*Cul-2*	GD 19297	wings disrupted	cell packing defect*
		GD 19298	wings disrupted	wild type
CG42616	*Cul-3*	GD 16331	wings disrupted	accumulation of Fmi
		NIG 11861R-1	wings disrupted	accumulation of Fmi
		NIG 11861R-2	wings disrupted	accumulation of Fmi
		KK 109415	wings disrupted	accumulation of Fmi
CG8711	*Cul-4*	NIG 8711R-1	wings disrupted	wild type
CG1401	*Cul-5*	GD 52175	wild type	wild type
		GD 52176	wild type	wid type
		KK 108817	lethal	wild type

GD, GD collection of RNAi lines from VDRC.
KK, KK collection of RNAi lines from VDRC.
NIG, RNAi lines from NIG-FLY.
Wings disrupted: hair polarity could not be assessed as wings could not be mounted flat.
Cell packing defect: cells not organised in the normal hexagonal array.
*Fmi asymmetric in hexagonal cells.

Table S4. Adult and pupal wing screen of genes encoding BTB domain proteins

CG number	Gene symbol	RNAi line	*MS1096-GAL4* adult wing	*ptc-GAL4* pupal wing
CG10465	CG10465	KK 107131	variable hair orientation	wild type
CG10752	CG10752	GD 30007	wild type	-
		NIG 10752R-1	wild type	-
		NIG 10752R-3	wild type	-
		KK 106721	wings disrupted	wild type
CG10801	CG10801	GD 45748	wild type	-
		GD 45749	wild type	-
		KK 100397	wings slightly disrupted, possible swirl	wild type
CG11275	CG11275	NIG 11275R-1	wild type	-
		NIG 11275R-2	wild type	-
CG11491	*br*	GD 13705	lethal	disrupted
		GD 38526	wings disrupted	wild type
		NIG 11514R-1	wild type	-
CG11714	CG11714	GD 31116	wild type	-
		GD 31117	wild type	-
		GD 50558	wild type	-
		GD 50559	wild type	-
CG12052	*lola*	GD 12573	wild type	-
		GD 20634	wild type	wild type
		GD 21057	wild type	-
		GD 25333	wings disrupted	wild type
		GD 41415	lethal	large cells
CG12236	CG12236	NIG 12236R-1	disrupted	large cells
CG12423	*klhl10*	GD 35721	wild type	-
		GD 35722	wild type	-
		KK 109083	wings disrupted	wild type
CG12537	*rdx*	GD 28798	wings disrupted	wild type
		GD 28800	wings disrupted	wild type
		GD 45759	wild type	-
		GD 45761	wings disrupted	wild type
CG12692	CG12692	GD 17292	wild type	-
		KK 109683	wild type	-
CG12857	CG12857	GD 45029	wild type	-
		GD 45030	wild type	-
		NIG 12857R-2	wild type	-
		NIG 12857R-3	wild type	-
		KK 101639	wild type	-
CG13917	CG13917	GD 32082	wings disrupted	cell packing defect
CG14260	CG14260	GD 50132	wild type	-
		NIG 14260R-4	wild type	-
CG14262	CG14262	GD 24855	wild type	-
		GD 24856	wild type	-
CG14307	*fru*	KK 105005	wings slightly disrupted, possible swirl, multiple wing hairs	wild type
CG14785	CG14785	GD 43594	wings disrupted	wild type

CG number	Gene symbol	RNAi line	*MS1096-GAL4* adult wing	*ptc-GAL4* pupal wing
CG15097	CG15097	KK 109428	wings slightly disrupted, possible swirl	slightly large cells
CG15725	CG15725	GD 38868	wild type	-
		KK 103687	wild type	-
		KK 106953	wild type	-
CG15812	*pfk*	GD 13361	wings disrupted	wild type
		GD 14020	wings disrupted	wild type
CG16778	CG16778	GD 10739	wild type	-
CG16952	CG16952	GD 10149	wild type	-
		GD 19166	wild type	-
CG17068	CG17068	GD 32849	wild type	-
		GD 32850	wild type	-
		NIG 17068R-1	wild type	-
		NIG 17068R-4	wild type	-
CG17754	CG17754	GD 47274	weak multiple wing hairs	wild type
		GD 47275	wild type	-
		GD 47276	wild type	-
		GD 47277	wild type	-
		KK 104337	wings disrupted	wild type
CG1812	CG1812	GD 15491	wild type	-
CG1826	CG1826	GD 33049	wild type	-
CG18471	*gprs*	GD 41673	wild type	-
CG1856	*ttk*	KK 10855	wild type	-
CG2368	*psq*	GD 30591	wild type	-
		KK 106404	wings disrupted	lethal
CG30357	CG30357	GD 21144	wild type	-
		KK 108708	wild type	-
CG31666	*chinmo*	NIG 17156R-1	vein defects	wild type
		NIG 17156R-2	variable hair orientation	-
CG32121	CG32121	GD 34404	wild type	-
		GD 34405	wings disrupted	cell packing defect
CG32491	*mod (mdg4)*	GD 52268	lethal	cell packing defect
		NIG 15802R-1	lethal	cell packing defect
		NIG 15802R-3	wild type	-
		NIG 32491R-1	wings disrupted	wild type
CG33261	*Trl*	GD 41095	wings disrupted	cell packing defect*
		NIG 9343R-1	hair morphology defect	wild type
		NIG 9343R-2	wings curly	slightly large cells
		KK 106433	wings disrupted	cell packing defect*
CG33291	CG33291	GD 35501	wild type	-
		GD 35503	wild type	-
		KK 107170	ectopic bristles	-

CG number	Gene symbol	RNAi line	*MS1096-GAL4* adult wing	*ptc-GAL4* pupal wing
CG34346	*mamo*	GD 29874	wild type	wild type
		GD 29875	wild type	wild type
		GD 38223	wings disrupted	wild type
		GD 45349	wings disrupted	cell packing defect
		GD 48679	wild type	-
		GD 48680	wild type	-
		NIG 11082R-2	wild type	-
		NIG 11082R-3	wild type	-
CG34376	CG34376	GD 24804	wild type	-
		GD 24805	wings disrupted	wild type
		GD 25038	wild type	-
		NIG 31160R-1	wild type	-
		NIG 31160R-3	wings disrupted	wild type
		KK 102795	wings disrupted	wild type
CG3571	*KLHL18*	GD 12052	wild type	-
		GD 43777	wild type	-
		GD 43778	wild type	-
CG3711	CG3711	GD 11164	wild type	-
		GD 11166	wild type	-
		NIG 3711R-2	wild type	-
		NIG 3711R-3	wild type	-
CG3726	CG3726	GD 41090	wild type	-
		GD 41091	wild type	-
CG3962	*Keap1*	KK 107052	wings curly	wild type
CG4069	CG4069	GD 21783	wings disrupted	wild type
CG41099	CG41099	GD 32927	wild type	-
		GD 32928	wild type	-
		GD 40076	wild type	-
CG43226	*lute*	GD 34986	wild type	-
		GD 34987	wild type	-
		NIG 5319R-3	wild type	wild type
		NIG 5319R-4	wild type	-
		KK 108082	disrupted	slightly large cells
CG43365	*BtbVII*	KK 106063	wings disrupted	cell packing defect
CG4807	*ab*	GD 41005	lethal	cell packing defect
CG5186	*slim*	GD 15185	wild type	-
		NIG 5186R-1	wild type	-
		NIG 5186R-2	wings disrupted	lethal
CG5575	*ken*	GD 48596	lethal	disrupted
CG5701	*RhoBTB*	KK 100815	wings disrupted	wild type
CG5738	*lolal*	GD 9571	lethal	lethal
		GD 9572	lethal	cell packing defect
		GD 9573	wings disrupted	cell packing defect
CG6118	CG6118	GD 38061	lethal	wild type
		GD 38062	lethal	wild type

CG number	Gene symbol	RNAi line	*MS1096-GAL4* adult wing	*ptc-GAL4* pupal wing
CG6224	*dbo*	GD 22476	wild type	wild type‡
		NIG 6224R-1	variable hair orientation	wild type‡
		NIG 6224R-3	variable hair orientation	wild type‡
		KK 105407	wings disrupted	slight accumulation of Fmi?‡
G6384	*Cp190*	GD 35077	wild type	-
		GD 35078	wings disrupted	wild type
		NIG 6384R-1	wild type	-
CG6758	CG6758	GD 43606	wild type	-
CG6765	CG6765	GD 22424	wild type	-
		NIG 6765R-1	wild type	-
		NIG 6765R-2	wild type	-
		KK 100851	wings slightly disrupted	wild type
CG6792	CG6792	GD 35118	vein defects	wild type
		GD 35119	wild type	wild type
		NIG 6792R-2	wild type	-
		NIG 6792R-3	wild type	-
CG7058	CG7058	GD 38230	wild type	-
		GD 38231	wild type	-
		NIG 7058R-1	wild type	-
		NIG 7058R-3	weak multiple wing hairs	-
CG7102	CG7102	GD 20571	wild type	-
		KK 107887	wings disrupted	wild type
CG7210	*kel*	KK 105397	wings disrupted	slight accumulation of Fmi?
CG7230	*rib*	GD 15900	wild type	-
		NIG 7230R-2	wild type	-
		NIG 7230R-4	wild type	wild type
		KK 103977	wild type	-
CG7837	CG7837	GD 22573	wild type	-
		GD 23099	wild type	-
		KK 109784	ectopic bristles	-
CG8060	CG8060	GD 22684	wild type	-
		GD 46990	wild type	-
		GD 46991	wild type	-
		NIG 8060R-1	wings disrupted	wild type
		NIG 8069R-2	wild type	-
CG8260	CG8260	GD 45257	wings disrupted	wild type
CG8411	*gcl*	GD 28896	wild type	-
		GD 28897	wild type	-
		NIG 8411R-2	wild type	-
		NIG 8411R-3	wild type	-
CG8811	*muskelin*	GD 29774	wild type	-
		KK 107043	wings disrupted	lethal
CG8924	CG8924	GD 48041	wild type	-
		GD 48042	wild type#	wild type
		NIG 8924R-1	wild type	-
		NIG 8924R-2	wild type	-

CG number	Gene symbol	RNAi line	*MS1096-GAL4* adult wing	*ptc-GAL4* pupal wing
CG9097	*bab1*	GD 6960	lethal	cell packing defect
		GD 6961	lethal	cell packing defect
		GD 24496	wild type	-
		GD 50285	wild type	-
		GD 50286	wild type	-
CG9102	*bab2*	GD 8943	wild type	-
		GD 49042	wild type	wild type
		GD 49043	wild type	-
CG9426	CG9426	GD 10843	wild type	-
		NIG 9426R-2	wild type	-
CG9467	CG9467	GD 45806	ectopic bristles	wild type
		GD 45807	wild type	-
CG9970	CG9970	GD 45817	wild type	-

GD, GD collection of RNAi lines from VDRC.
KK, KK collection of RNAi lines from VDRC.
NIG, RNAi lines from NIG-FLY.
Wings disrupted: hair polarity could not be assessed as wings could not be mounted flat.
Cell packing defect: cells not organised in the normal hexagonal array.
Irregular cells: cell size and packing disturbed.
[#]Using *ptc-GAL4*.
*Fmi asymmetric in hexagonal cells.
[‡]Strong accumulation of Fmi in combination with *kel*$^{IR\text{-}JF01768}$. Note that the hairpins in the existing RNAi lines targeting *dbo* all overlap.

Table S5. Summary of epistasis experiments

	Ubc12$^{IR\text{-}30033}$	*Cul-3*$^{IR\text{-}109415}$	*faf*$^{IR\text{-}2956}$
wt	Fmi Fz Stbm Pk Dsh strong increase	Fmi Fz Stbm Pk Dsh strong increase	Fmi Fz Stbm Pk Dsh strong decrease
fz^{P21}	Fmi Stbm Pk slight increase	Fmi Stbm Pk wild type levels	Fmi Stbm Pk strong decrease
stbm^{6}	Fmi Fz Dsh slight increase	Fmi Fz Dsh slight increase	Fmi Fz Dsh strong decrease
pk$^{pk\text{-}sple13}$	Fmi Fz Stbm Dsh strong increase	Fmi Fz Stbm Dsh strong increase	Fmi Fz Stbm Dsh strong decrease
dgo^{380}	Fmi Fz Stbm Dsh strong increase	Fmi Fz Stbm Dsh strong increase	Fmi Fz Stbm Dsh strong decrease
dsh^{V26}	Fmi (wt) Stbm (wt) wild type levels*	Fmi Stbm wild type levels	Fmi Stbm strong decrease

ptc-GAL4 was used to express RNAi against *Ubc12*, *Cul-3* or *faf* in the various mutant backgrounds, and the levels of junctional proteins were assessed relative to non-RNAi-expressing tissue within the same wing. The table shows all the core proteins that were tested for any particular genotype. If a protein is not listed, this indicates that its junctional levels were not analysed in this genotype.
*Distal *dsh* clones within the *Ubc12* RNAi-expressing domain completely suppress the accumulation of core proteins at junctions caused by the RNAi, as the RNAi expression is less well expressed distally. Proximal *dsh* clones (in regions where the *Ubc12* RNAi is strongly expressed) do not completely suppress the accumulation phenotype. This argues that *Ubc12* has a second target that affects core protein accumulation at junctions.